(12)

AD

ON THE ORIGIN AND EVOLUTION OF THREE DIMENSIONAL EFFECTS IN THE MIXING LAYER

Final Technical Report

by

Javier JIMENEZ

Rodrigo MARTINEZ-VAL

Manuel REBOLLO

Laboratory of Fluid Mechanics, School of Aeronautics

Universidad Politécnica de Madrid

Madrid - 3 (SPAIN)

December, 1979

EUROPEAN RESEARCH OFFICE

United States Army

London England

GRANT NUMBER DA-ERO 78-G-079

Excmo. Sr. D. Jose Luis Ramos Figueras

Rector Magnífico de la Universidad Politécnica

Cea Bermúdez, 10, Madrid - 3 (SPAIN)

UNCLASSIFIED

SECURITY CLASSIFICATION OF THIS PAGE (When Data Entered)

R&D 2572 MC/AN

REPORT DOCUMENTATION PAGE

READ INSTRUCTIONS BEFORE COMPLETING FORM

1. REPORT NUMBER	2. GOVT ACCESSION NO. AD-A096 007
	3. RECIPIENT'S CATALOG NUMBER
4. TITLE (and Subtitle) On the Origin and Evolution of Three Dimensional Effects in the Mixing Layer.	5. TYPE OF REPORT & PERIOD COVERED Final Technical Report. Jul 78 – 9 Jul 79
	6. PERFORMING ORG. REPORT NUMBER
7. AUTHOR(s) Javier Jimenez, Rodrigo Martinez-Val, Manuel Rebollo	8. CONTRACT OR GRANT NUMBER(s) DAERO-78-G-079
9. PERFORMING ORGANIZATION NAME AND ADDRESS Laboratory of Fluid Mechanics, School of Aeronautics, Universidad Politecnica de Madrid, Spain	10. PROGRAM ELEMENT, PROJECT, TASK AREA & WORK UNIT NUMBERS 6.11.02A.1T161102BH57-06
11. CONTROLLING OFFICE NAME AND ADDRESS US Army R&S Gp (Eur), Box 65, FPO NY 09510	12. REPORT DATE Dec 79
	13. NUMBER OF PAGES 60
14. MONITORING AGENCY NAME & ADDRESS (if different from Controlling Office)	15. SECURITY CLASS. (of this report) Unclassified
	15a. DECLASSIFICATION/DOWNGRADING SCHEDULE

16. DISTRIBUTION STATEMENT (of this Report)

Approved for Public Release; Distribution Unlimited

17. DISTRIBUTION STATEMENT (of the abstract entered in Block 20, if different from Report)

18. SUPPLEMENTARY NOTES

19. KEY WORDS (Continue on reverse side if necessary and identify by block number)

Instability of 2-D Turbulence
Mixing Layers and Coherent Structure
Streaks
Ejections

20. ABSTRACT (Continue on reverse side if necessary and identify by block number)

There seems to be at least two different phenomena connected with the three-dimensional breakdown of the plane mixing layer. First, at least in some cases, there is a macroscopic instability of the large structure which produces a spanwise system of longitudinal jets whose amplitude builds up very quickly and then remains approximately constant while their separation adjust itself to a value that is somewhat higher that the vorticity thickness of the layer. This phenomenon may be due to a collective instability of the vortex cores of the same type as the one found in vortex

DD FORM 1 JAN 73 1473 EDITION OF 1 NOV 65 IS OBSOLETE

UNCLASSIFIED

SECURITY CLASSIFICATION OF THIS PAGE (When Data Entered)

20. Contd.

rings.

The second phenomenon is the development of a 3-D inertial subrange in the spectrum of the small scales of the velocity fluctuations. In the only case in which we have documented both phenomena the second one does not develop fully until the macroscopic instability has not been growing for some time and has actually arrived to what seems to be its final configuration.

Moreover there is some indication that there are two qualitatively different ways for the establishment of the 3-D inertial ranges, examplified here by the water and air experiments. In the first one the transition is abrupt and there is an initial part in which the inertial range has a slope characteristic of the 2-D enstrophy cascade. In the second one the transition is more gradual and there is no evidence of a 2-D regime. It is not clear at present which is the condition responsible for the differences between the two cases.

The work presented in this report should be seen as a preliminary exploration of the effects connected with the 3-D transition. Much more research is needed is all cases.

AD

ON THE ORIGIN AND EVOLUTION OF THREE DIMENSIONAL EFFECTS IN THE MIXING LAYER

Final Technical Report

by

Javier JIMENEZ

Rodrigo MARTINEZ-VAL

Manuel REBOLLO

Laboratory of Fluid Mechanics, School of Aeronautics

Universidad Politécnica de Madrid

Madrid - 3 (SPAIN)

December, 1979

EUROPEAN RESEARCH OFFICE

United States Army

London England

GRANT NUMBER DA-ERO 78-G-079

Excmo. Sr. D. Jose Luis Ramos Figueras

Rector Magnífico de la Universidad Politécnica

Cea Bermúdez, 10, Madrid - 3 (SPAIN)

ABSTRACT

The transition to three-dimensionality in a plane mixing layer is studied through exploration of the flow field and analysis of the power spectrum of longitudinal velocity fluctuations.

Two different phenomena are identified. First the appearance of 3-D small scale fluctuations is marked by the transition of the slope of the inertial subrange towards the value of -5/3. Second we find in one case that the large scale itself shows an instability, with wavelengths of the order of the vorticity thickness of the layer, and that seems to be explained by a collective "corrugation" of the vortex cores. This second phenomena is studied in some detail.

TABLE OF CONTENTS

1. INTRODUCTION

It is generally agreed that three-dimensionality is an essential property of fully developed turbulence. Even if 2-D turbulence is possible it is only under three-dimensional conditions that a fully developed energy cascade is established and leads to the production of enough small scale motion to account for the rapid mixing of concentration and momentum gradients that is characteristic of turbulent flows.

The plane mixing layer is a well studied flow in which the initial conditions are two-dimensional and the flow remains two-dimensional for a long time after separation. In fact there is evidence that the large scales of the flow may stay two-dimensional essentially forever [1,2]. Since it is obvious that the small scale motion in the mixing layer should, and indeed does, eventually become three-dimensional, this flow is a good test case to study the instabilities that are responsible for the breakdown of two-dimensional motion.

This transition has been studied previously by various investigators from several points of view. Bradshaw [3] measured the evolution of the turbulence level in the mixing layer and its approach to its equilibrium value. Perhaps significantly this approach was found to depend on whether the initial boundary layer was turbulent or laminar and thus, possibly, on the amount of initial three- dimensionality in the flow. The evolution of the turbulence level has been measured more recently by other investigators for different initial conditions [4,5] but it is still not clear whether the establishment of three-dimensionality coincides with the attainment of the equilibrium value of the fluctuation intensity.

More recently Konrad [6] and Breidenthal [7] have identified a transition in the amount of molecular mixing present in a two-species shear layer. Since enhanced mixing must come from an increase of small scale structure this transition is probably associated with the onset of three-dimensinality [8].

We have used still another property, the evolution of the slope of the inertial subrange of the longitudinal velocity power spectrum towards its 3-D value of -5/3, as an indicator of three-dimensionality. The transition is clearly visible in the three cases that we have studied and is discussed in section 5.

Another interesting and related problem is the possible appearance of three-dimensionality in the large structures, as opposed to the small scales. Chandrsuda et. al. [9] reported helical distorsion of the vortices in a plane mixing layer and similar effects have been described in the

initial region of circular jets [10]. Konrad has reported the appearance of longitudinal streaks in his concentration pictures and Breidenthal has associated these streaks with sinusoidal corrugations of the vortex cores. In one of our flows, the only one checked for detailed spanwise structure, we have found permanent longitudinal jets that may correspond to the same effect and seem to be associated to, although they precede, the transition to small scale three-dimensionality. These results are described in section 6.

Some of our measurements were carried out with hot film anemometers in water. Since that technique is not too well developed a significant amount of time was spent checking and improving the accuracy of the method, and the results are briefly discussed in section 3.

Due to the time limitations involved in this study many of the experiments presented are exploratory and many of the conclusions tentative. Further work is being carried out to confirm and extend them.

2. FLOW FACILITIES AND EQUIPMENT

The experiments have been performed in two independent facilities: a water tunnel and 2-D air half-jet.

Water Tunnel

The experimental apparatus is basically a blow-down tunnel in which a plane mixing layer is established between two streams of water coming from two large independent reservoirs (figure 1). Both tanks are pressurized with air at 1.5 kg/cm^2 to keep the change in velocity, due to the drop in water level throughout the shot, below a maximum of .5%.

The two streams go through a conventional sequence of control valves, flow-meters, settling chamber, straightners and screens and a 4:1 contraction before they are brought into contact to form a plane mixing layer at the exit ot two 7.5 x 15 cm nozzles in the test section, from where they are discarded through a siphon.

The test section is 15 x 15 cm across and 100 cm long. In the lateral walls there are three pairs of registers which, together with a sliding probe holder, allow manual positioning of the probe at any downstream coordinate up to 40 cm from the edge of the splitter plate. Cross-stream probe motion is achieved by means of a traversing gear which incorporates a stepping motor, with a .2 mm step, and is controlled by a HP 2100S minicomputer which automatizes the water experiments.

Although the apparatus can provide a flow with temperatures as well as velocity differences, the experiments reported in this work have been conducted in a homogeneous shear layer.

A steady flow is established in less than a second at nominal velocities of 19 and 37 cm/s. Under these conditions the momentum thickness of both boundary layers, at the end of the splitter plate, are .7 and .5 mm respectively. A waiting time of about 15 s is needed before the water initially in the settling chamber is swept completely and the temperature is uniform enough to allow the use of hot film sensors. With this in mind, maximum useful running time is about 50 s.

We have run performance tests on the apparatus and the free stream turbulence level was found to be about .2%. The free stream velocities were found repeatable for 100 different shots and constant throughout a given one to within .5%. The shear across the central part of the free stream high velocity side was less than .2% and of the order of 1% in the low velocity side.

Even if the tanks are thermally insulated it is unavoid-

able to have some temperature difference between them. This difference is monitored by means of thermistors and can be kept below .1 °C which represents a velocity error of about .2%.

Air Half Jet

The air flow facility was used during the last part of the experiments. A blower-tunnel was utilized to supply a two-dimensional mixing layer in air. A blowing fan powered by a 3.7 Kw, 2870 rpm motor supplied the air flow through a diffuser to a plenum chamber. The plenum chamber contained foam, screens and a deep honeycomb in order to reduce the turbulence level at the nozzle exit. The air was exhausted through a rectangular nozzle of 7x13 cm (figure 2.). The contraction ratio was 10:1.

The jet was allowed to mix on one of its boundaries with the surrounding quiescent air, the other three being solid to prevent the formation of mixing layers.

A traversing gear provides three degrees of freedom with a precision of .05 mm in the x-y plane and .2 mm in the spanwise direction.

The maximum velocity could be as high as 50 m/s although all the experiments in air have been performed at 25 or 16.6 m/s. A more detailed description of this facility is given in section 6.

Anemometry and Data Acquisition System

Velocity measurements were carried out in both mixing layers with a DISA 55D01 anemometer in constant temperature mode without linearization. The output of the anemometer was fed into a 10 bit HP5610A analog-digital converter and the digitized data were stored by the HP 2100S minicomputer in magnetic tape. Data rate was governed by an independent programmable crystal clock which provided a stable frequency standard. The tape thus produced was then processed off-line in a large IBM 370/158 computer.

In the water tunnel facility the experiments were controlled by the HP 2100S that opened and closed the valves, moved the probe and monitored such ancillary data as tank temperature, flowmeter output and probe position.

3. MEASUREMENT TECHNIQUES

Hot Film Anemometry in Water

The velocity measurements in water were carried out using a hot film quartz coated single sensor DISA 55A81 wedge probe. Probe overheat was kept at .05, which gave us enough sensitivity while minimizing the risk of bubble formation and deposition of dirt on the probe surface [11]. Even at this low overheat, and even if we filtered our water through a 3 μm filter to minimize the number of nucleation points, bubbles were present (see figure 3) and about 10% of the runs had to be discarded because of this problem.

Surface contamination produced a day to day drift in the thermal characteristics of the film which caused a change in the calibration curve. To study this effect we calibrated our probe in a small, low speed recirculating tunnel with very low turbulence level, in which the velocity was measured simultaneously with the probe and with a calibrated flowmeter placed in the recirculating duct. The upper part of figure 4 shows different calibrations, carried out on different days and showing clearly the drift. To correct this effect we tested several heat transmission models based on the expression

$$Nu_c = Nu - \beta Nu^n \qquad (3.1)$$

where Nu is the Nusselt number as actually measured by the probe, Nu_c is the corrected Nusselt number that would be measured by an ideal uncontaminated film and β is a parameter related to the ratio of thermal conductances of the coating and the fluid that must be found empirically for each calibration. A detailed account of this method can be found in [12]. There we find that the best collapse of the data happens for n=2 (see figure 5) in agreement with the model proposed by Morrow and Kline in [13]. Applying this correction to the calibration data, all points fall close to the "ideal" curve that is shown in the lower part of figure 4. The standard deviation with respect to this curve decreases from 8% before correction to 1.6%.

The application of this correction model to experimental situations presents additional problems, since at least the real velocity at one point has to be known to compute β. Diaphragm flowmeters were introduced in the supply lines to monitor the volumetric flows but, since the test section walls were fixed and we expected some pressure gradient to develop on the streamwise direction, these flows gave us only the velocity at the exit of the nozzles. In fact the pressure gradient had to be computed as part of the probe calibration procedure.

Let us assume that one data point is measured in each stream giving Nusselts Nu_1 and Nu_2 and that the velocities at the exit of the nozzles are known to be U_{1E} and U_{2E}. The velocities in the sections under consideration can be related to the pressure through Barnouilli's equation which after linearization gives,

$$U_i = U_{iE} - \Delta p/\rho U_{iE} \tag{3.2}$$

If the calibration formula for the probe is

$$U = f(Nu_c) = f(Nu - \beta Nu^2), \tag{3.3}$$

linearizing again and substituting in (3.2) we get from the two streams a system of linear equations permitting us to compute β and the pressure as functions of the measured Nusselt numbers and velocities at the nozzle. Figure 6 shows the pressure gradient computed in this way in five different co-ordinates along the test section, confirming the consistency of the above procedure and the applicability of the correction method.

Taking into account the scatter and errors associated with the calibration of the probe, the flowmeters and the measurements of water temperature and pressure gradient we estimate the accuracy of our velocity measurements to be approximately 3%.

Hot Wire Measurements in Air

In the mixing layer in air classical hot wire anemometry techniques were applied. Velocity fluctuations were measured with a DISA 55F31 hot wire probe, 5 μm in diameter and 1.25 mm in length. An overheat ratio of 0.8 was used in all cases.

Data processing

Two different types of data were taken during the water tunnel experiments: a) profile measurements at four downstream sections and b) spectral measurements at fixed positions within the shear layer.

Ten to twelve points were taken in each traverse. The data collection period per point was 3 seconds which corresponds to approximately 10 large structures passing by at the most downstream section, x=37 cm.

The spectral measurements were taken leaving the probe standing still at fixed positions within the layer and, in order to resolve very low frequencies, the data collection period at these points was the whole duration of the run, i.e. 40 to 50 seconds.

In the air experiments the measurements taken were essentially the same, although the exploration was extended to three dimensions, and the data collection period was changed to correspond to the different frequencies involved.

Mean and rms velocities in water were computed by using the calibration curve on the digital data, and taking the average and standard deviation of the resulting velocity records. Our previous knowledge of the free stream velocities, the pressure gradient and the hot film drift was used in this reduction.

The spectra, both in air and water, were also computed in this way. The mean velocity was removed for each run, and an averaged FFT technique [14], with a Blackmann-Harris data window [15], was used to obtain the power spectra. Finally all the spectra correspoding to a given station were averaged together. Since the length of a long run is 40 to 50 s and 4 to 6 runs were made on every single point the minimum number of large structures presented in each averaged spectrum is close to 1000, although in some cases it is much larger.

Mean quantities in air were averaged analogically from the anemometer output and later reduced to velocity and turbulence levels.

4. RESULTS

Flow description: water

The top part of figure 7 shows nondimensional profiles of mean velocity which fit fairly well to an error function curve. In spite of the slight favourable pressure gradient mentioned above the growth is linear and similarity is achieved. The vorticity thickness of the layer was measured and the spreading rate found to be .0793, with a virtual origin located 26 mm upstream of the splitter plate edge. This spreading rate is perhaps a little high but within the range of values given in previous studies [16], [17]. The dividing streamline is $\eta = -.0065$ where the nondimensional mean velocity is $(U-U_2)/(U_1-U_2)=.58$.

The bottom part of the figure presents the rms value of longitudinal velocity fluctuations at two sections. In the most upstream one some influence of the initial conditions can still be detected and the general turbulence level is higher than in the other one. The Reynolds numbers for both sections, $x\Delta U/\nu$, are 34000 and 63000 which are below the limits given in [3] and [10] as needed to attain similarity of the fluctuation profiles. In fact figure 9 shows the maximum value of fluctuations measured as a function of downstream coordinate and it is clear that it has not yet attained its equilibrium value. This asymptotic value can be estimated to be between .18 and .19 which is again a little high but reasonable. The facts that both the growth rate and the turbulence level are slightly high might not be independent [18].

Some time lapse pictures of the shear layer were taken by injecting dye at the splitter plate and these pictures were used to measure the visual spreading rate. The resulting value $\delta/(x-x_0)=.125$ is consistent with that given in [19], even if it is not clear whether dye visualization should give the same spreading rates as the shadowgraphs.

Flow description: air

A study of the two-dimensional air half jet was undertaken with the splitter plate of type I of figure 2 , which is essentially a thin aluminium sheet and a jet velocity of 25 m/s. The mixing layer thus formed has been analyzed through mean and fluctuation velocity profiles and spectra taken at several positions.

The top of figure 8 presents nondimensional profiles of mean velocity, which fit fairly well to the expected error function curve. From these profiles we see that similarity has been attained at least since x=80 mm. The vorticity thickness of the layer was measured and the spreading rate

was found to be .195, with a virtual origin located 9 mm upstream of the splitter plate edge. This spreading rate is half way between those reported by Wygnansky and Fiedler [20] and Liepmann and Laufer [21]. The dividing streamline is $\eta_0 = .03$ and the corresponding non-dimensional mean velocity is $(U-U_2)/(U_1-U_2) = .57$. This result is the same as the one found in [21].

The bottom part of figure 8 shows the rms value of longitudinal velocity fluctuations at three sections. The most upstream profile indicates that the turbulent intensity has not achieved its equilibrium value, and this is confirmed in figure 14. The asymptotic value of the maximum $u'/\Delta U$ is .17 which again agrees fairly well with those reported in [20] and [21].

A third experiment using the same facility and a velocity of 16.4 m/s is described in section 6.

5. SPECTRAL RESULTS

In order to study the development and interaction of the large coherent structures and their possible relation to the origin and evolution of three-dimensionality we have carried out a detailed spectral analysis of the velocity fluctuations in our three mixing layers: the two-stream water facility and the air half-jet at two different velocities.

All spectra were taken at the mid-span plane. Those in water were measured either at $\eta = y/(x-x_0) = 0$ or $\eta = .043$. The last position permitted a reliable detection of the large structure peaks, not yet swamped by the strong low-frequency noise that seems to be associated to the center of the mixing layer, while still showing a high-frequency inertial subrange characteristic of fully turbulent flow. A typical evolution of the power spectra across the mixing layer is shown in figure 10.

For the high-speed air jet (25m/s) all spectra were taken at $\eta = 0$ while those for the low speed one (16.4 m/s) fall in two series, none of them along a similarity ray. One series was measured at $U/U_\infty = .5$ and was used to study the inertial subranges while the other, at $U/U_\infty = .08$ and therefore in the outer edge of the layer, was used for the detection of the large structures. Since this work is related to mixing layer transition and most of the data are far from the asymptotic similarity range, this later approach was found more satisfactory than keying the measurements to geometric variables that are relevant mostly for the downstream, well developed, part of the layer.

The frequency behaviour of the spectra can be divided broadly into three ranges: low frequencies, large structures and inertial range. Only the last two are studied separately below since the low frequency one, though interesting [22], does not seem to be influenced by three-dimensionality.

The spectrum of the large eddies

The part of the spectrum corresponding to the large structures is the most interesting one but also the most complex as can be seen in figure 11, which shows the downstream evolution of the water spectra.

One of the most noticeable aspects is the existance of peaks which can be followed across several stations with a very definite constant frequency, while the low frequency ones gain importance as we move downstream. The evolution of the position of these peaks with downstream coordinate is given in the bottom part of figures 12-a,b and c, for the three layers. For the purpose of these figures a peak was included if its maximum power was at least 10% above the spectral continuum at that frequency.

An important phenomenon is that the ratio between successive spectral lines is mostly two, although different factors, like 1.5, are also present. These values agree with those given by Hernan and Jimenez [23] and Jimenez et al. [22] and can be explained by means of the amalgamation process. The doubling is easy to understand through the coallescence of two equal eddies. The factor 1.5 is also explained assuming the amalgamation between structures of two successive generations, which implies that some eddies of the last one have escaped without pairing and hence coexist and eventually amalgamate with vortices whose scales are twice as large.

The same variables are shown nondimensionalized in figure 13. The frequencies are made non-dimensional with the convection velocity, $\bar{U}=U_1+U_2/2$, and with a characteristic lenght which is supposed to be proportional to the wavelength of the initial instability of the layer. For the air jets this length is the momentum thickness, δ_2, of the boundary layer [3, 19]; for the water layer we have used an equivalent thickness, related to the most unstable wave length of the wake profile of the splitter plate (see Appendix A). The longitudinal coordinate is made non-dimensional with the length $\bar{U}\delta_2/\Delta U$, proportional to the length needed for a spatially amplified disturbance to develop [24].

In these dimensionless variables the frequencies of most spectral peaks agree for the three mixing layers, especially near the splitter plate, indicating that instability theory dominates the flow for at least a few pairings. Those spectral peaks which appear only in one of the layers can usually be traced to forcing frequencies, e.g. blower frequency, which are not intrinsic to the flow. Moreover, in the downstream region in which some degree of self-preservation has been achieved, all layers follow a unique frequency law which can be written as

$$\lambda = .3\ \Delta U\ x/\bar{U} \qquad (5.1)$$

and agrees very well with the data reported by other investigators [25,26].

Some coupling between the coherent structures and the instabilities of the initial boundary layer in the air experiments is apparent in that frequency peaks that will later be dominant in the mixing layer are visible very early in the downstrem development (fig. 12-b,c). The boundary layers in these cases are marginally unstable ($U\delta_1/\nu = 650$ and 520), and some of the frequencies induced either by the blower fan or possibly by coupling with downstream structures are amplified and seem to survive in the mixing layer. Other frequencies which are far from the

instability region in the boundary layer do not survive and are lost quickly, even if their absolute amplitude is larger (see also figure 16 and discussion in section 6). In the water mixing layer the boundary layers at both sides of the plate are stable ($U\delta_1/\nu < 450$) and the flow is "cleaner" than in the air jets.

The inertial subrange

All the spectra in figure 10, at different transverse positions, show an inertial subrange with a slope of -5/3; those in figure 11, taken at various downstream stations, also show the same slope, except the one taken at x=150 mm which is much steeper, close to -3. Since -5/3 is associated to the three-dimensional energy cascade the study of this subrange can be used to detect the outset of threedimensionality.

The upper parts of figures 12-a,b and c present the slopes of the inertial subranges in all those stations in which it could be measured with some confidence. It can be seen that the behaviour of the experiments in air and water is quite different. The water flow (figure 12a) presents a relatively sharp evolution from a slope of -3 to -5/3. The value of -3 is associated to the vorticity cascade which is normally assumed to control two-dimensional turbulence [27], and this suggests that the observed transition separates a situation in which velocity fluctuations are predominantly two-dimensional, even in the small scales, from one in which 3-D fluctuations become important. The change of slope occurs in a region in which several scales of coherent structures co-exist (see bottom of figure 12a) implying that the flow is more disordered there than in other zones.

The mixing layer of the air experiments do not show any evidence of a plateau near the slope of -3 and their approach to -5/3 is more gradual. Since the turbulence level in the free stream of this facility was somewhat higher (1%), and the boundary layers more unstable, the origin of three-dimensionality could be governed by different causes than in the water flow. In fact the situation is somewhat reminiscent of the behaviour of the maximum turbulence level in layers in which the initial conditions are laminar or turbulent [3, 4].

Figure 14 shows the slopes and the maximum turbulence levels for the three layers in terms of the same non-dimensional coordinate used for the spectral peaks. Two facts can be seen in this figure. First the transitions in water happens sooner and is indeed sharper than the one in air. This is again consistent with the idea that initial turbulence tends to retard transition. Second the approach to three-dimensionality is not completed until the velocity

fluctuations begin to decrease to their asymptotic level, confirming that the two phenomena are not unrelated.

The high frequency end of the inertial range is marked by a corner in the spectrum beyond which the slope becomes much steeper. The position of the corner is given in the bottom parts of figures 12a,b,c and is very near in all cases to the inverse of the sensor length, so that the new range is probably explained by the limitations of the sensing equipment.

Finally a word must be said concerning the dimensionless variables used. Considering that only three independent experiments are available it is not really possible to decide in most cases which is the appropriate normalization and the variables have been chosen with some particular theoretical model in mind. The growth of the large structures is the best understood process and consequently the non-dimensionalization works best in that case (figure 13). The cause of the three-dimensionality is less clear and we have done little else than trying several normalizing factors. Using as abcissa the ratio x/δ_2 gave slightly better results than the one used here, but was difficult to justify theoretically for the two-stream case. The obvious parameter , $\Delta U\ \delta_\omega/\nu$, increased the differences between the three experiments to almost an order of magnitude.

6. SPANWISE FLOW STRUCTURE

An important question is whether the transition to three-dimensionality is itself two-dimensional. An obvious possibility, for example, is that perturbations are injected from the end plates that limit the shear layer in span, and this mechanism has been shown to be important in some cases of transition in the two-dimensional wake behind a cylinder [28]. If this be so in our case it should be expected that the three-dimensionality will appear further upstream as we approach the end plates and, to test this hypothesis, we have explored the flow in a shear layer along the z coordinate as well as in the x-y plane. The somewhat surprising results are presented in this section.

Experimental arrangement.

The measurements were carried out in the air half jet adjusted to a nominal velocity of 16.4 m/s. Two slightly different splitter plate configurations were used which are shown in outline in figure 2. Cronologically, configuration I was used first and later taken appart and substituted by configuration II. The boundary layer in both cases was laminar with a momentun thickness of about .2 mm at the exit section, corresponding to an effective lenght of flat plate of 90 mm in case I, and slightly less in case II. This thickness was both computed from the area distribution of the exit nozzle and measured directly by exploration of the flow with a hot wire just downstream of the plate edge. When severe spanwise nonuniformities in the flow were discovered in shear layer I the two-dimensionality of the edge was checked and found to have irregularities with an amplitude of nearly .5 mm and a characteristic wavelength of 50 mm. Also a slight wobble (.2 mm) was found in the y position of the probe as it was traversed in the z direction. As a consequence, and even if it was doubtful whether such smooth irregularities could cause the observed effects, the splitter plate was substituted by a carefully machined square prism (II) whose two-dimensionality is thought to be better than .1 mm in the 130 mm span. The traversing mechanism was also rebuilt to minimize the wobble and any remaining deviations were calibrated against the edge of the splitter plate. This calibration procedure was repeated several times and the resulting positional accuracy of the probe with respect to the plate edge was estimated to be about .05 mm(rms). The x and y movement of the probe was done by a pair of crossed lathe beds whose positional resolution is also .05 mm, which probably accounts for much of the uncertainty quoted above. The data reported in this section refer to layer II unless explicity stated otherwise.

A general sketch of the nozzle geometry, together with the coordinate system used and the the approximate position of the mixing region is also shown in figure 2.

All measurements were taken with a single hot wire 1.25 mm long and 5 μm in diameter, whose holder, with a diameter of 3 mm, was held at an angle of 45 degrees out of the plane of the flow to minimize interference. The wire itself was aligned parallel to the splitter plate edge.

The spanwise uniformity of the free stream was checked and found to be better than .5%. The residual deviations were smooth and showed no sign of oscillatory behaviour. The free stream was 2% faster near the splitter plate than at the center of the jet in a way consistent with the expected flow at the exit of a concentration. The level of longitudinal velocity perturbations in the stream was comparatively high (.8%) and concentrated in a few well defined frequencies, mainly harmonical of the rotation frequency of the blower fan (48 Hz), and as a consequence, the boundary layer contained a rather high level of perturbations (4%). Power spectra for the free stream and boundary layer longitudinal velocities are given in figure 16 and show a clear correspondance between the important peaks in both cases. The frequencies of these peaks are also plotted on the Tollmien-Lin stability diagram for the instability limit for two-dimensional perturbations [29] and those peaks at the approximate frequencies show signs of slight amplification. Although no measurements were taken of the mechanical vibrations of the splitter plate it was clear by feeling manually the side walls of the tunnel that part of the perturbations to the boundary layer were transmitted that way, and by taking a series of steps to change the rigidity and mass of the tunnel walls the level of perturbations was reduced from about 10% to the final 4%.

The boundary layer, measured just downstream of the splitter plate, was not very two-dimensional. Four profiles are given in figure 17 in which the transverse coordinates have been normalized with the local measured momentum thickness. The average velocities are seen to collapse satisfactorily and to follow quite closely the Blasius profile for the laminar layer, but the turbulence levels show a large scatter. Figure 18 shows the spanwise variation of the momemtum thickness and the maximum turbulence level across half of the total span. The momentum thickness shows variations of almost 20% and the non-uniformity of the turbulence level is even higher. It is not clear which is the cause of this nonuniformity although it is presumably connected either with small geometric irregularities in the nozzle walls or with changes in the amplitude of the mechanical vibrations. The fact that the layer is just transitional probably amplifies the effect of any such perturbations.

The measurements were done over a period of several days and enough points were re-checked to make sure that the effect was repeatable and that the position of the nonuniformities remained constant with time, but no detailed comparison was done between the two splitter plate configurations and it is not known which was the effect of rebuilding the plate on the boundary layer.

Results

Most of the results presented in this section refer to average properties integrated analogically over periods of about one minute and reduced to velocity without making any allowance for effects due to hot wire nonlinearity. An exception is the data used in power spectra, which were digitized directly and treated in the way described earlier in the report. Each spectrum derives from about 400 s of measurements.

Using splitter plate I, we took data at two different spanwise locations, mid-span (z=0) and z=35 mm. Average longitudinal velocities and turbulence levels corresponding to the mid-span position are shown in figure 19 where the transverse coordinate is made nondimensional with the local computed vorticity thickness and normalized to the local central streamline, defined as the point where $U=.5\ U_\infty$. It is seen that the profiles become self similar beyond x=60 mm, and that this is true even for the turbulence levels, although with a larger scatter.

A less reassuring view is presented in figure 20 where the growth of the vorticity thickness and the evolution of the maximum turbulence levels are given for three cases, the two spanwise locations in layer I and the mid-span position of layer II. It is specially interesting to note that the growth of the thickness of layer I is not the same, even at the most downstream coordinate, for the two spanwise locations, and that the data for the other configuration do not agree either with any of the two curves, even if the three asymptotic growth rates are within the range of values found by other investigators.

As a consequence of this result the nozzle configuration was rebuilt and a detailed spanwise exploration of layer II was undertaken. Figure 21 shows the turbulence levels measured on the plane y=-.082(x-3.45 mm), and it is clear that, also in this case, there are spanwise nonuniformities amounting to nearly 15% of the average turbulence level and that these nonuniformities organize themselves broadly in long longitudinal streaks.

The next three figures show maps of average velocities and turbulence levels in three roughly orthogonal sections of the shear layer. Figure 22 is a conventional x-y map

taken at mid-span and shows the expected velocity distributions. In particular the peak that appears near x=30 mm in the turbulence level seems to be characteristic of flows with a laminar initial boundary layer [3].

The other two figures are spanwise sections and are constructed in a slightly different way. For each x-y position a representative value of velocity and turbulence level is defined by averaging over the spanwise coordinate, z, and the figures show the difference between actual measured properties and those locally constructed averages; they represent the effect of spanwise nonuniformities independently of the general background levels of the velocity and turbulence fields.

The x-z section in figure 23 shows clearly the streamwise turbulence streaks. The corresponding average velocity map shows that these streaks are associated to long streamwise jets of higher than normal velocity. The jets appear to attain their full strength near x=40 mm and are involved later in a series of interactions that keep increasing their separation progressively, although discontinuously, without appreciably decreasing their intensity.

The transversal structure of these streaks is shown in the y-z section in figure 24 where the jets are shown to have transversal as well as longitudinal coherence. Perhaps the most significant feature in this figure is that the velocity field is roughly simmetrical about the central streamline, while the turbulence level is approximately antysimmetrical. This is in contradiction with the explanation of the nonuniformities as streamwise vortices of the type postulated by Benney [30] and known to be important in the transition of the laminar boundary layer, and agrees more with a model involving streamwise jets, or cross-stream vortices. This will be discussed later in more detail.

In understanding these jets an obvious possibility is that they are somehow inherited from some irregularity in the initial conditions. We saw before that the free stream in the neighbourhood of the splitter plate was examinated and shown to be uniform within the accuracy of the hot wire equipment, but that the spanwise nonuniformities found in the boundary layer just after separation were important enough to be considered as likely candidates to be the cause of the stronger features found further downstream.

Before this matter is examined a word must be said regarding the accuracy of the measurements. It was noted above that the position of the probe was known only to within .05 mm and, since near the splitter plate there are strong transverse velocity gradients, this uncertainty induces errors in the measurement that can be important in the upstream part of the layer. These errors are large enough that data on velocity variations upstream of x=15 mm

are not really significant and could be consistent with a uniform average velocity while turbulence data, being less affected by strong gradients, are qualitatively, although not quantitatively, reliable all the way to the splitter plate.

Having in mind this warning, the x-z map in figure 23 suggests that there is no direct continuity between the features in boundary layer and those downstream. In particular the region between x=5 and 20 mm seems to be one of reorganization of the spanwise structure, while the fact that the separation of the jets changes downstream and that there is a rapid increase in their intensity near x=40 mm suggests that some kind of local instability of the mixing layer is responsible for them.

If we think of the large coherent eddies of the mixing layer as representative of the dominant longitudinal mode of layer instability, the spanwise nonuniformities can be considered as a secondary wave superimposed on that main one, and by comparing the power spectra of the flow at various z positions it should be possible to study the properties of that wave.

For a particular x-y position we define a reference turbulence level $\overline{\sigma^2} = \overline{u'^2}$ and power spectrum $\bar{P}$ by averaging over the span. At a given z the deviations from these values can be ascribed to the secondary spanwise wave and, to a first approximation, we could expect that the deviation in the spectra are proportional to those in σ^2. If this is true the normalized excess power spectrum

$$p(f,z) = \frac{P(f,z) - \bar{P}(f)}{\bar{P}(f)} \frac{\overline{\sigma^2}}{\sigma^2(z) - \overline{\sigma^2}} \qquad (6.1)$$

should be independent of z and represent the frequency structure of the secondary wave. Figure 25 shows an estimate of this quantity for three different x-y points, obtained by evaluating equation (6.1) at several spanwise positions and averaging over z,

$$\hat{p}(f) = \langle p(f,z) \rangle_z \qquad (6.2)$$

Since the integral of the power spectrum should equal σ^2 it is easy to see that $\hat{p}$ should, in the average, be equal to 1, with those frequencies where $\hat{p}>1$ representing the spectral peaks associated with the secondary wave. The main peaks evident in the spectra in figure 25 are represented in the lower part of the figure superimposed on the x-frequency diagram that gives the evolution of the large structure in the layer (see also figure 12-c). If the jets were just

"fossil" effects deriving from activity in the boundary layer one would expect their spectral behaviour to remain constant downstream, with peaks associated either to the spanwise instabilities of the transitional boundary layer [31] or with the forcing frequency from the blower fan. Instead, the dominant frequency shifts downstream and remains locked approximately with the frequencies associated to the large eddies in the mixing region. This gives further support to the view that the streaks are caused by an intrinsic local instability.

A final piece of evidence, although fragmentary and difficult to interpret, is important enough that it should be presented here. Before the apparatus for layer I was taken apart and the exit nozzle rebuilt, some exploratory measurements were taken of the spanwise distribution of velocity and turbulence. Since it was expected that the reworking of the splitter plate, with its complete change in the position and nature of all random irregularities, would change also the nonuniformities in the flow, no measurements were taken for layer II at the same points as in I. Nevertheless the measurements taken in I are represented in figure 26 together with their closest equivalent in II. While the most upstream data do not show any similarity in both cases, due may be as much to the inaccuracy of the measurements in that station as to anything else, the situation is different in the downstream sections where the similarities are high enough that it is difficult to escape the conclusion that the two flows have basically the same spanwise structure.

Since there is a very low probability that the spanwise structure of the initial boundary layer is even roughly similar in both cases, the similarity of the final flow seems to imply that the initial conditions are not important for the development of spanwise nonuniformities. Whether this persistance of the structure after the reworking of the splitter plate is due to some intrinsic property of the layer or to an irregularity of the free stream, not the boundary layer, small enough to be undetectable by our equipment but still important for the flow is not clear and must await further investigation.

Theoretical considerations

We have shown that under some conditions a mixing region that should be expected to be two-dimensional contains a definite three-dimensional structure consisting of high turbulence streaks associated to high velocity longitudinal jets. The position of these streaks remains fairly constant from one day to another and even shows some degree of permanence after severe changes in the initial conditions.

Similar three-dimensional effects have been observed in other flows, notably in the transitional boundary layer [31] and in the wake behind a two-dimensional body [28]. In the mixing layer Konrad [6] observed longitudinal streaks in the concentration interface while Breidenthal [7] repeated the observation under different conditions and showed that the streaks arise from "corrugations" in the vortex cores of the large structure.

Benney [30] studied theoretically the nonlinear development of the instability of a laminar mixing layer and concluded that a three-dimensional wave can interact with the dominant three-dimensional mode to produce permanent three dimensional variations of average velocity associated to longitudinal vortices aligned with the x-axis. That work was aimed at explaining the transition in the laminar boundary layer, where longitudinal vortices are known to appear, but unfortunately does not explain the transversal structure of the streaks observed in our case.

In fact a longitudinal vortex transfers momentum accross the mixing layer producing an average antysimmetric distribution of velocity excess, in contradiction with the results presented in figure 24.

The structure shown in that figure suggest that the vortices responsible for the streaks are aligned in the transverse, y, direction, while the spectral results show that these vortices are somehow in phase with the large structure. When the two results are put together we arrive at a picture in which the vortex cores of the primary two-dimensional instability are deformed or corrugated in accordance with Breidenthal's pictures, and the corrugation has at least a component in the y-z plane. At the points where the corrugation is concave towards the high velocity side the velocity is higher while the center of the core, and therefore the region of higher turbulence, is displaced towards the low speed side of the layer (see figure 27). This picture is in qualitative agreement with the data in figure 24 but, if these features are to be visible in the average, all the cores have to deform "in step".

Saffman [32] has suggested that the instability responsible for the corrugation of the cores is the same one appearing in vortex rings. Briefly, the criterion for instability is that a core deforms in such a way that its self-induced rotational speed is zero [33], in which case the strain field induced by other cores in the layer is able to pull it appart and feed the growth of the deformation. This growth starts at an angle of 45 degrees to the flow direction and has therefore the transverse component implied by our observations.

The lowest mode for which this happens is a corrugation of the core in which both radial and spanwise vorticity

distributions are changed. The most unstable wavelength depends on the vorticity distribution assumed initially within the cores but it falls between 2 and 2.5 times the vortex radius [34, 35], and, if we estimate this radius as about half the vorticity thickness of the layer we arrive at

$$\lambda \sim 1 \text{ to } 1.25\ \delta_\omega \tag{6.3}$$

While this is only a rough estimate, the wavelengths measured in the layer and shown in figure 28 are indeed of this order of magnitude, specially in the downstream part of the layer where the streak system is well developed. Thus, this mechanism might be able to explain the instability of a single vortex core, but the question of whether it is possible to lock all the vortices in the layer into a coherent instability that will produce the observed jets is still open and needs further investigation.

7. CONCLUSIONS

There seems to be at least two different phenomena connected with the three-dimensional breakdown of the plane mixing layer. First, at least in some cases, there is a macroscopic instability of the large structure which produces a spanwise system of longitudinal jets whose amplitude builds up very quickly and then remains approximately constant while their separation adjust itself to a value that is somewhat higher that the vorticity thickness of the layer. This phenomenon may be due to a collective instability of the vortex cores of the same type as the one found in vortex rings.

The second phenomenon is the development of a 3-D inertial subrange in the spectrum of the small scales of the velocity fluctuations. In the only case in which we have documented both phenomena the second one does not develop fully until the macroscopic instability has not been growing for some time and has actually arrived to what seems to be its final configuration.

Moreover there is some indication that there are two qualitatively different ways for the establishment of the 3-D inertial ranges, examplified here by the water and air experiments. In the first one the transition is abrupt and there is an initial part in which the inertial range has a slope characteristic of the 2-D enstrophy cascade. In the second one the transition is more gradual and there is no evidence of a 2-D regime. It is not clear, at present, which is the condition responsible for the differences between the two cases.

An interesting coincidence is that in the three cases studied here, the transition to three-dimensionality in the small scales happens near the second or third vortex amalgamation (see figures 12-a,b and c), despite differences of one order of magnitude between the Reynolds numbers involved. It may be that the amalgamations act as trigger for the transition, but the small number of cases makes it impossible again to derive definitive conclusions.

We believe the work presented in this report should be seen as a preliminary exploration of the effects connected with the 3-D transition. Much more research is needed in all cases. In particular it is important to check whether the spanwise macroscopic breakdown can be reproduced in different circumstances and how it depends on initial conditions and Reynolds number. An interesting question, in view of the importance of 3-D structure for a vigorous mixing, is whether this instability can be enhanced and used to shorten the distance needed for transition in practical flows.

Secondly the influence of vortex amalgamations on transition should be checked. Again more experiments with

different initial conditions are needed for this, but the tools developed in this study using the power spectra of velocity fluctuations should be enough to detect both the average position of the pairings and the position of three-dimensional breakdown.

We want to acknowledge the support of part of this investigation by the Spanish Comision Asesora de Investigacion as well as the help of the UAM-IBM Scientific Center in Madrid which gave us access to its computer center for the digital processing of the data in this report.

APPENDIX A

Stability characteristics of the splitter plate wake.

The wavelength of the initial instability in a mixing layer is strongly influenced by the wake of the splitter plate in those cases in which both free stream velocities are different from zero. The downstream distance needed for viscosity to fill the dip in the profile produced by the initial boundry layers is of the order of the equivalent flat plate length of those layers while the amplification distance for the unstable disturbances is proportional to the layer thickness and is usually much smaller. Moreover, for the commonly found Reynolds numbers the wake flow is unstable from the moment it leaves the splitter plate and the nonlinear regime of the instability is achieved before any appreciable evolution of the profile has taken place.

It seems likely therefore that the wavelength of the initial instability is fixed by the initial wake profile and we present here an analysis of a simple straight line approximation to this profile. Approximation of this type have been shown to be useful in other cases [36, 37] and give a quantitative basis for comparison between different profiles. In particular the variation of wavelengths between different velocity ratios should be given approximatly by this model.

The profile we use is shown in figure 29. If we introduce a perturbation stream function

$$\Psi(x, y, t) = \Psi(x, y) + \Phi(y)\ \exp(i\alpha(x-ct)), \qquad (A.1)$$

and assume infinite Reynolds number and parallel flow, the perturbation amplitude satisfies the equation [38],

$$(U - c)(\Phi'' - \alpha^2\Phi) - U''\Phi = 0. \qquad (A.2)$$

In the segments in which U is linear the solution of (A.2) is given by

$$\Phi \sim \exp(\pm\ \alpha y), \qquad (A.3)$$

while at the corners, where U" is infinite, the stream function remains continuous but the derivatives satisfy a jump condition

$$\Phi'_+ - \Phi'_- = \Phi(U'_+ - U'_-)/(U-c) \qquad (A.4)$$

When we add the conditions that Φ remains bounded at infinity and assuming that the real part of α is positive, the solution of (A.1) can be divided in the segments shown in

figure 29. The jump conditions give relations between the various coefficients, and the final result is a cubic eigenvalue equation to be satisfied by c.

In the case of the mixing layer the equivalent flat plate length for both boundary layers is usually the same, and the thickness are related by

$$h_2/h_1 = (U_1/U_2)^{1/2} \qquad (A.5)$$

The solutions to the eigenvalue equation with this condition is given in figure 30, where the stability boundary is given in terms of the wave number and the velocity ratio, together with isolines of the spatial amplification rate $\alpha h_1 c_i/c_r$. The properties of the most amplified wave are also given in figure 31 as functions of the velocity ratio.

For our water mixing layer $U_2/U_1 = .51$ and the most unstable wave number is 1.25 times that of the half jet with the same boundary layer thickness at the high speed side. Therefore the wavelength and the "equivalent" initial thickness can be taken as .8 times the real high speed side value, which is the thickness used in section 5.

Some of the ideas presented in this appendix where suggested by Prof. A. Liñan.

REFERENCES

1. Dimotakis P.E. and Brown G.L. (1978). The mixing layer at high Reynolds numbers. J. Fluid Mech., 78, pp. 535-560.

2. Wygnanski I., Oster D., Fiedler H. and Dziomba B. (1979). On the perseverance of quasy-two-dimensional eddy-structure in a turbulent mixing layer. J. Fluid Mech., 93, pp. 325-335.

3. Bradshaw P. (1966). The effect of initial conditions on the development of the free shear layer. J. Fluid Mech., 26, pp. 225-236.

4. Hussain A.K.M.F. and Zedan M.F. (1978). Effects of the initial condition on the axisymmetric free shear layer: Effects of the initial momentum thickness. Phys. Fluids, 21, pp. 1100-1112.

5. Crow S.C. and Champagne F.H. (1971). Orderly structure in jet turbulence. J. Fluid Mech., 48, pp. 547-591.

6. Konrad J.H. (1977). An experimental investigation of mixing in two-dimensional turbulent shear flows with applications to diffusion- limited chemical reactions. Ph. D. Thesis. California Institute of Technology.

7. Breidenthal R.E. (1978). A chemically reacting, turbulent shear layer. Ph. D. Thesis, California Institute of Technology.

8. Bernal L.P., Breidenthal R.E., Brown G.L., Konrad J.H. and Roshko A. (1979). Proc. 2nd Symp. on Turbulent shear Flows, London, pp. 8.1 - 8.7.

9. Chandrsuda C., Mehta R.D., Weir A.D. and Bradshaw P (1978) Effect of free-stream turbulence on large structure in turbulent mixing layers. J. Fluid Mech., 85., pp. 693-704.

10. Yule A.J. (1978). Large scale structure in the mixing layer of a round jet. J. Fluid Mech., 89. pp. 413-432.

11. Rasmussen C.G. (1967). The air bubble problem in water flow hot film anemometry. DISA Information, 5, pp. 21-22.

12. Jimenez J., Martinez-Val R. and Rebollo M. (1979). Hot film sensors calibration drift in water. Submitted to J. Physics E.

13. Morrow T.B. and Kline S.J. (1974). The performance of hot wire and hot film anemometers in water. Flow: its measurement and control, (R.E. Wendt Ed.), Instrument Society of America. Pittsburg, Penn.

14. Welch P.D. (1967). The use of FFT for the estimation of power spectra. IEEE Transactions Audio Electroacustics, 15, pp. 70-73.

15. Harris F.J. (1978). On the use of windows for harmonic analysis with DFT. Proc. IEEE, 66, pp. 51-83.

16. Mills R.D. (1968). Numerical and experimental investigations of the shear layer between two parallel streams. J. Fluid Mech., 33, pp. 591-616

17. Miles J.B. and Shih J. (1968). Similarity parameter for two-stream turbulent jet mixing region, AIAA Journal, 6. pp. 1429-1430

18. Pui N.K. and Gartshore I.S. (1979). Measurements of the growth rate and structure in plane turbulent mixing layers. J. Fluid Mech., 91. pp. 111-130.

19. Roshko A. (1976). Structure of turbulent shear flows: a new look, AIAA Paper 76-78.

20. Wygnanski I. and Fiedler H.E. (1970). The two dimensional mixing region. J. Fluid Mech., 41, pp. 327-362.

21. Liepmann H.W. and Laufer, J. (1947). Investigation of free turbulent mixing. NACA Tech. Note 1257.

22. Jimenez J., Martinez-Val R. and Rebollo M (1979). The spectrum of large scale structures in a mixing layer. Proc. 2nd Symp. on Turbulent Shear Flows. London, pp. 8.7-8.12.

23. Hernan M.A. and Jimenez J. (1979). The use of digital image analysis in optical flow measurements. Proc. 2nd Symp. on Turbulent Shear Flows. London, pp. 7.7-7.14.

24. Jimenez J. (1980). On the visual growth of a turbulent mixing layer. J. Fluid Mech., 96, pp. 445-458.

25. Brown G.L. and Roshko A. (1974). On density effects and large structure in turbulent mixing layers. J. Fluid Mech., 64, pp. 775-816.

26. Winant C.D. and Browand F.K. (1974). Vortex pairing: the mechanism of turbulent mixing layer growth at moderate Reynolds numbers. J. Fluid Mech., 63, pp. 237-255.

27. Batchelor G.K. (1969). Computations of the energy spectrum in homogeneous 2-D turbulence. Phys. Fluids Suppl. II, pp. 233-239.

28. Garrard J.H. (1966). The three-dimensional structure of the wake of a circular cylinder. J. Fluid Mech., 25, pp 143-164.

29. Shen S.F. (1954). Calculated amplified oscillations in plane Poiseuille and Blasius flows. J. Aero. Sci., 21, pp. 62-64.

30. Benney D.J. (1961). A non-linear theory for oscillations in a parallel flow. J. Fluid Mech., 10, pp. 209-236.

31. Klebanoff P.S., Tidstron K.D. and Sargent L.M. (1962). The three-dimensional nature of boundary layer instability. J. Fluid Mech., 12, pp. 1-34.

32. Saffman P.G. and Baker G.R. (1979). Vortex interactions. Ann. Rev. Fluid Mech., 11, pp. 95-122.

33. Windnall S.E., Bliss D.B. and Tsai C.-Y. (1974). The instability of short waves in a vortex ring. J. Fluid Mech., 66, pp. 35-47.

34. Tsai C.-Y. and Widnall S.E. (1976). The instability of short waves in a straight vortex filament in a weak externally imposed strain field. J.Fluid Mech., 73, pp. 721-733.

35. Saffman P.G. (1978). The number of waves on unstable vortex rings. J. Fluid Mech., 84, pp. 625-639.

36. Esch R.E. (1957). The instability of a shear layer between two parallel streams. J. Fluid Mech., 3, pp. 289-303.

37. Michalke A. and Schade H. (1963). Zur Stabilitat von freien Grenzschichten. Ing. Archiv., 33, pp. 1-23.

38. Lin C.C. (1955). The theory of hydrodinamic stability. Cambridge Univ. Press. Cambridge. England.

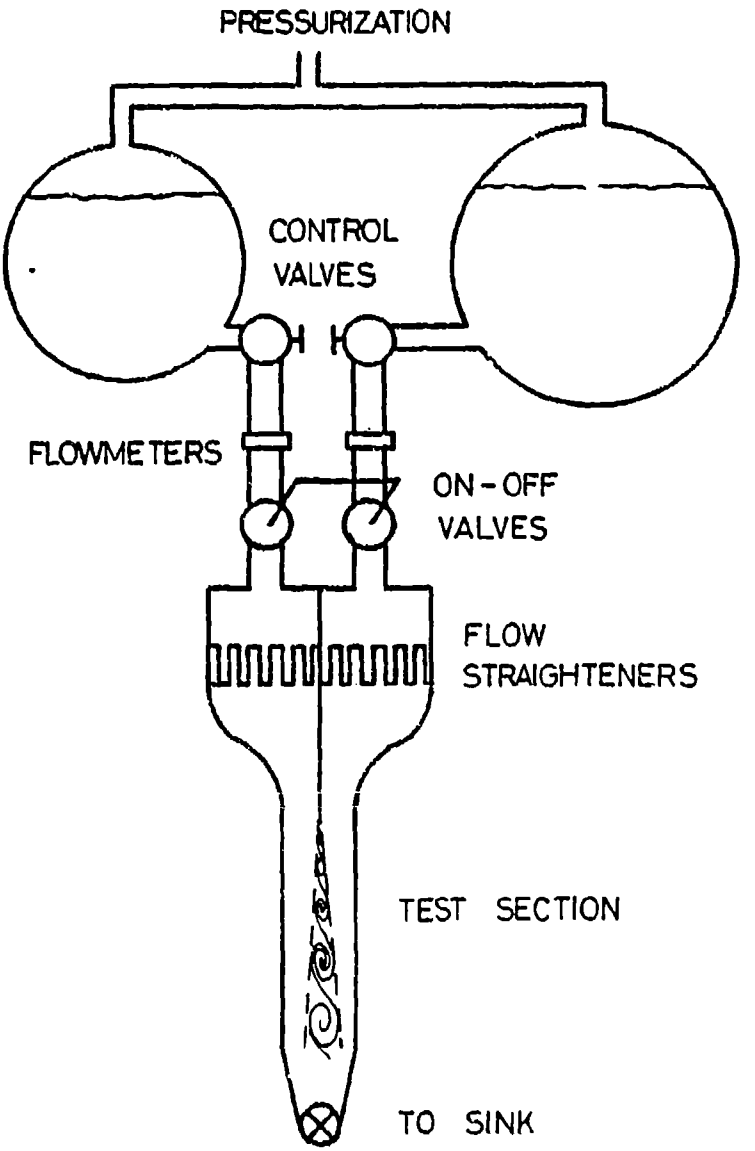

Fig. 1.- Schematic view of water installation.

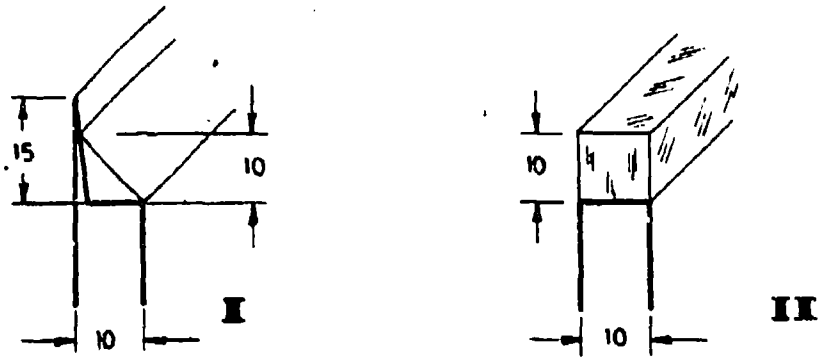

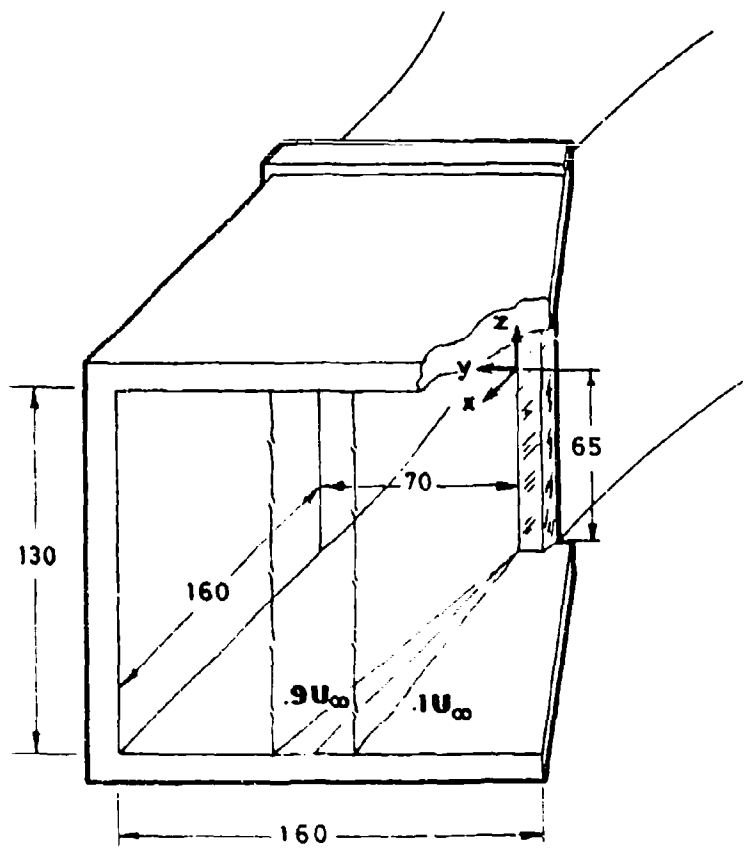

Fig. 2.- Geometry of test section in air half-jet. Two splitter plates were used which are represented on top. Coordinate system shown is that used in section 6 of text.

Fig. 3.- Effect of an air bubble in the voltage response of the hot film sensor.

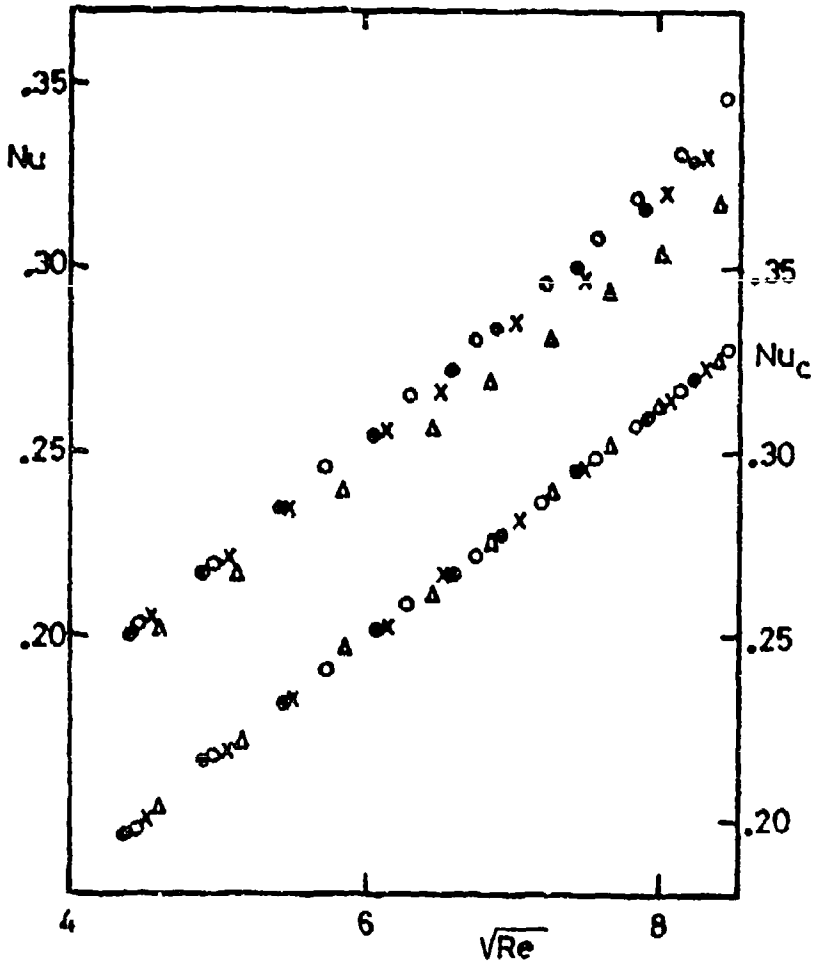

Fig. 4.- Four different hot film calibrations showing drift (top), and "ideal" curve obtained through correction (3.1) with n = 2.

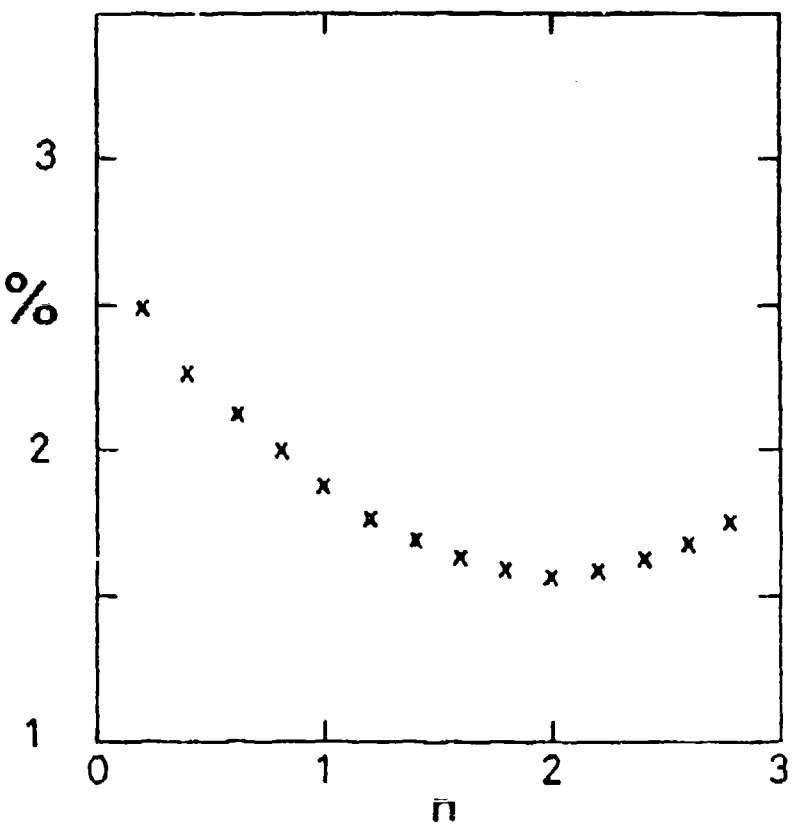

Fig. 5.- Variation of rms error after correction of calibration drift as a function of the exponent in equation (3.1).

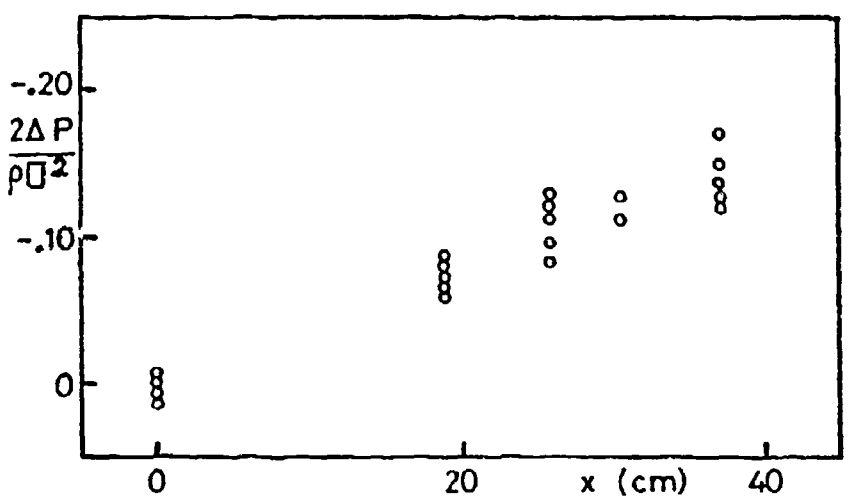

Fig. 6.- Pressure gradient in test section of water tunnel computed as part of the drift correction procedure for the hot film.

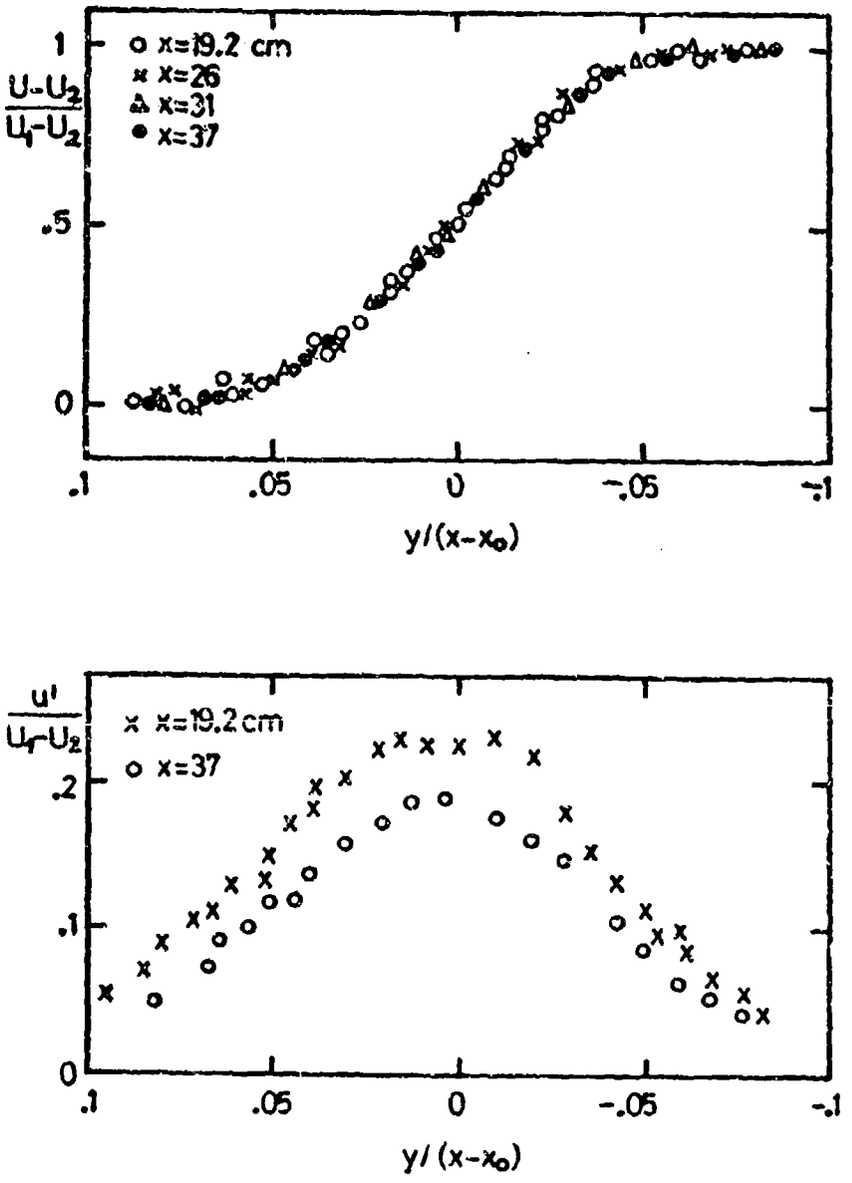

Fig. 7.- Average velocity (top) and fluctuation profiles for the water mixing layer; U_2/U_1=.51.

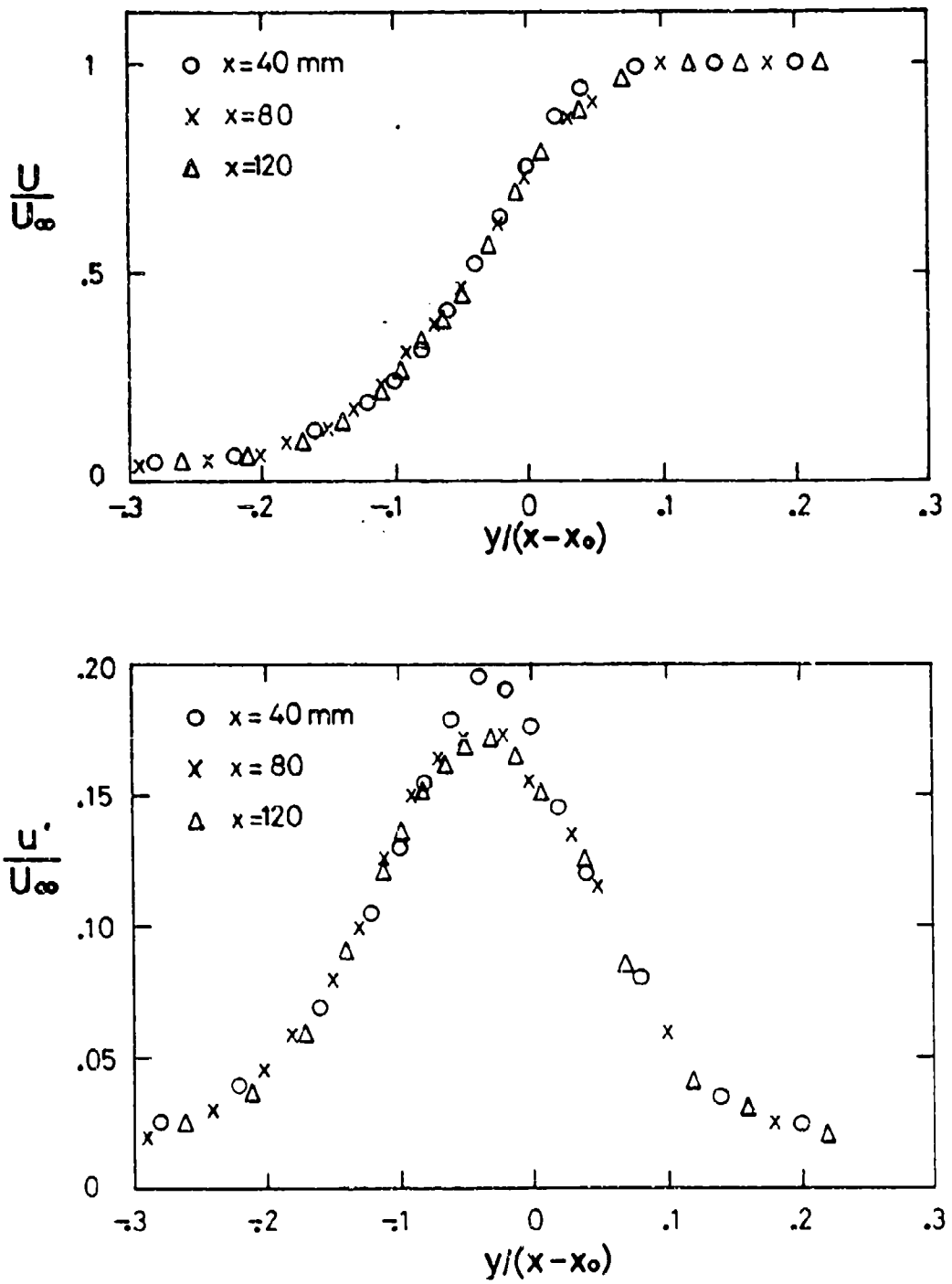

Fig. 8.- Average velocity (top) and fluctuation profiles for the air half-jet (U_∞ = 25 m/s).

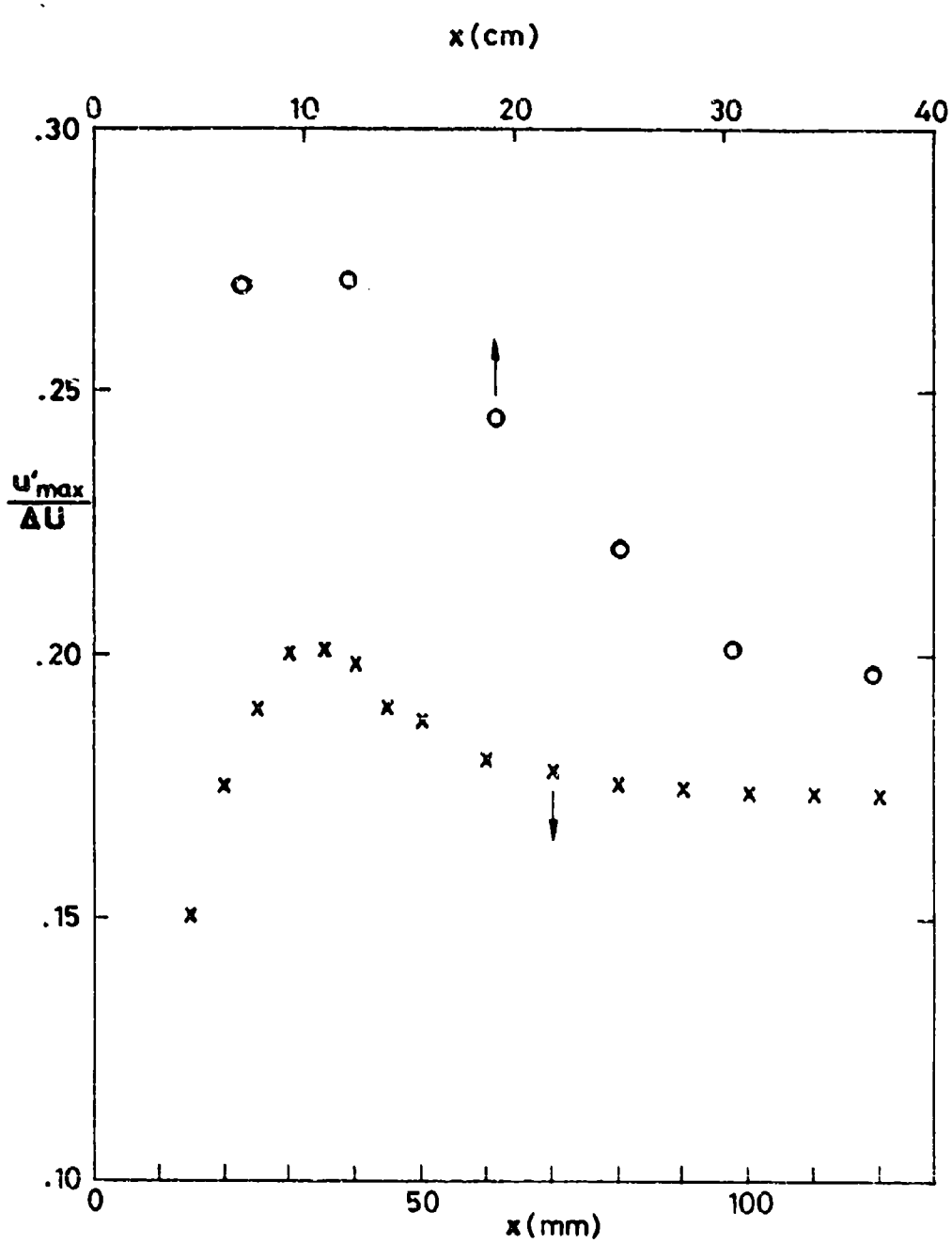

Fig. 9.- Variation of turbulence level with downstream coordinates. O, water layer, top abcissae; X, air (25 m/s) bottom.

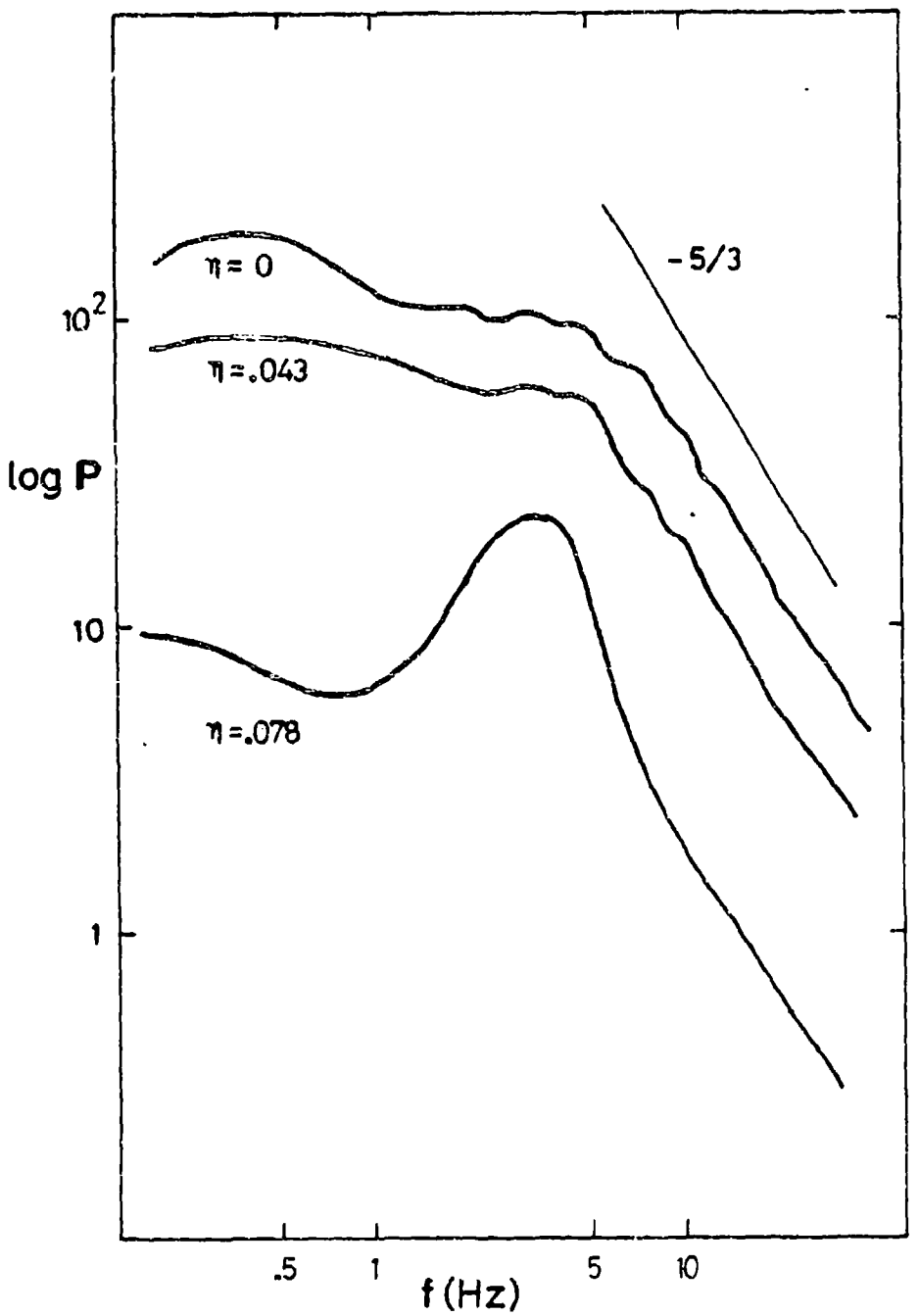

Fig. 10.- Evolution of power spectra accross mixing layer in water. $U_2/U_1 = .51$; x = 250 mm.

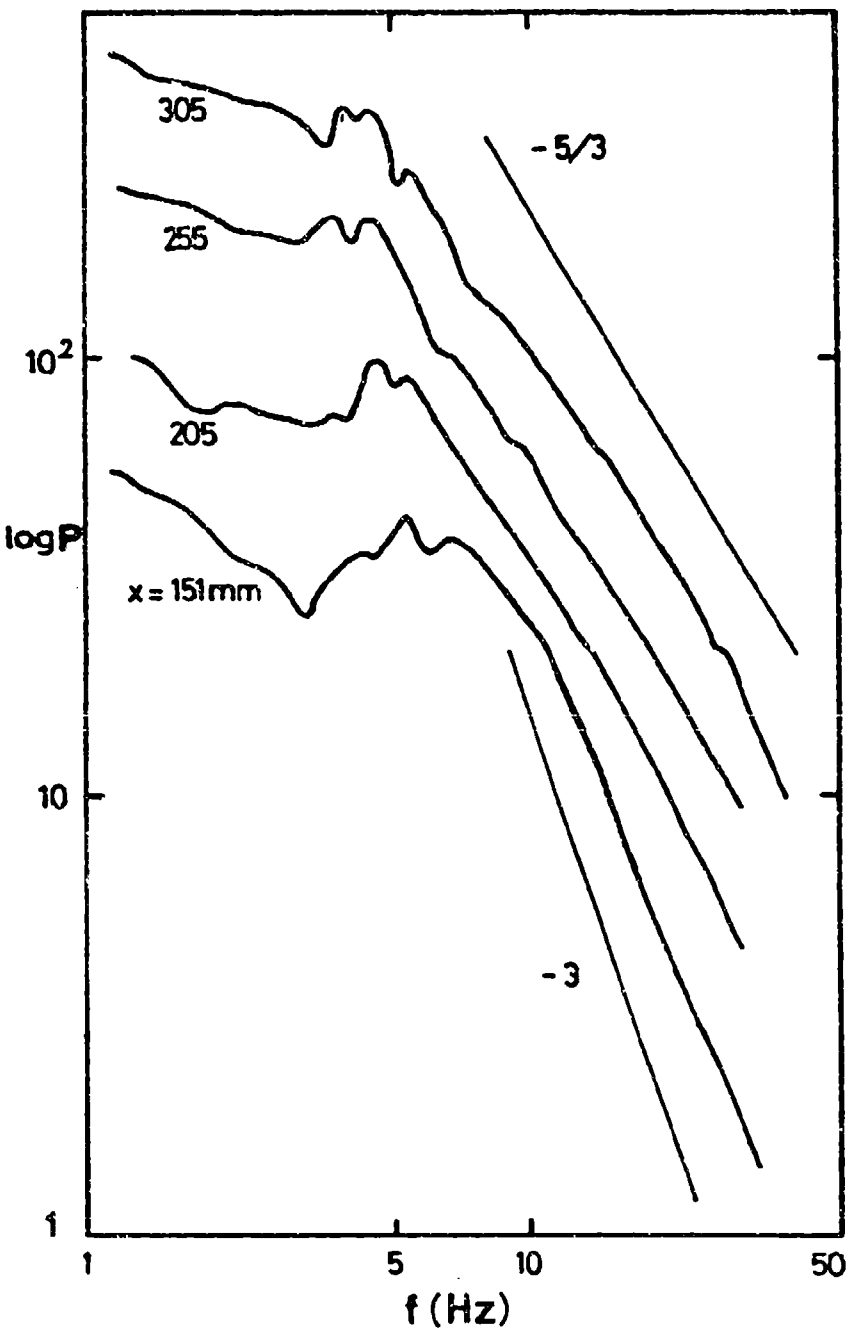

Fig. 11.- Power spectra variation with downstream coordinate. Water layer at n = .043.

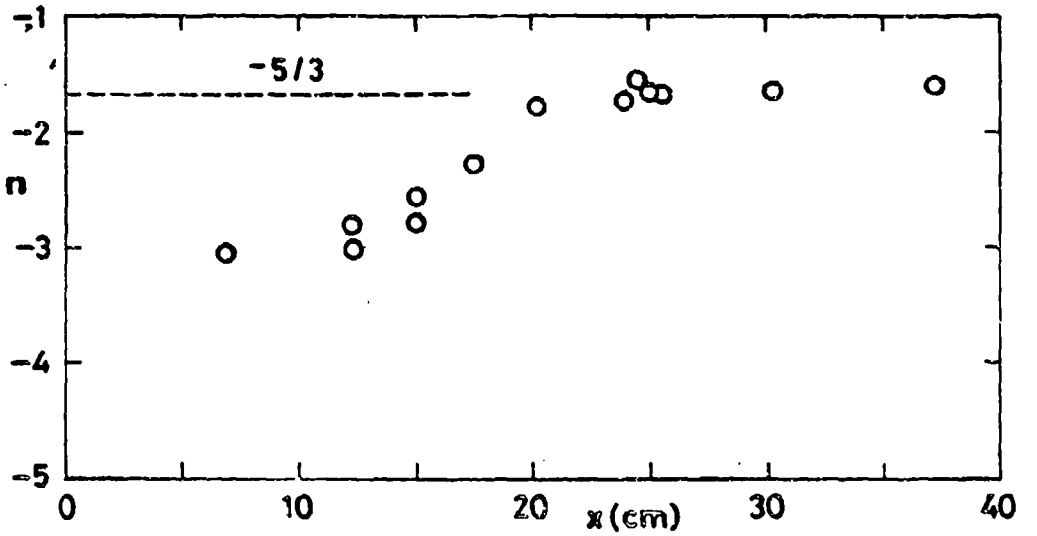

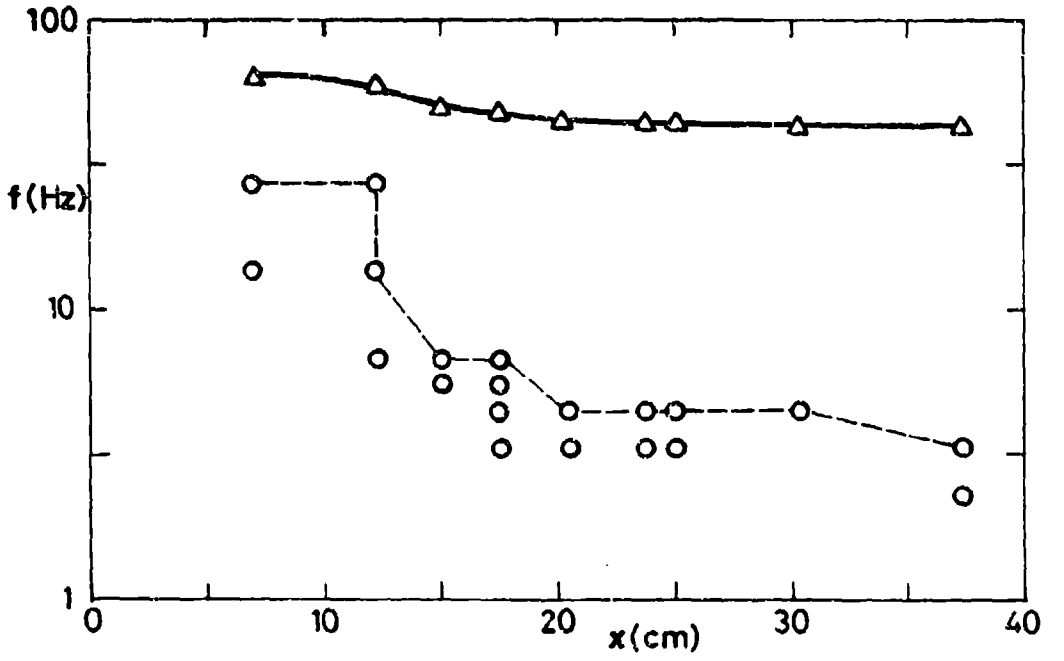

Fig. 12a.- For legend see page 43.

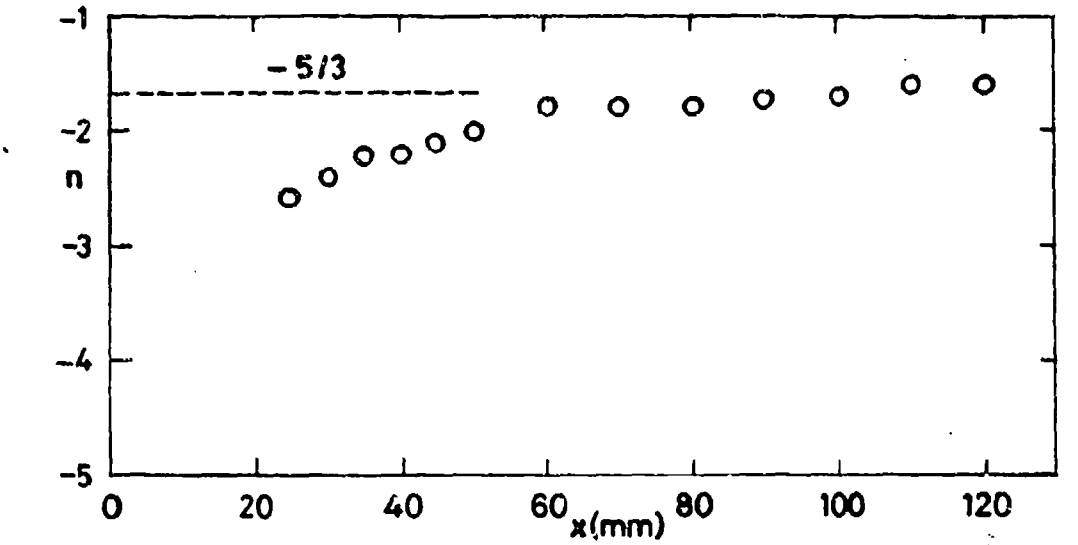

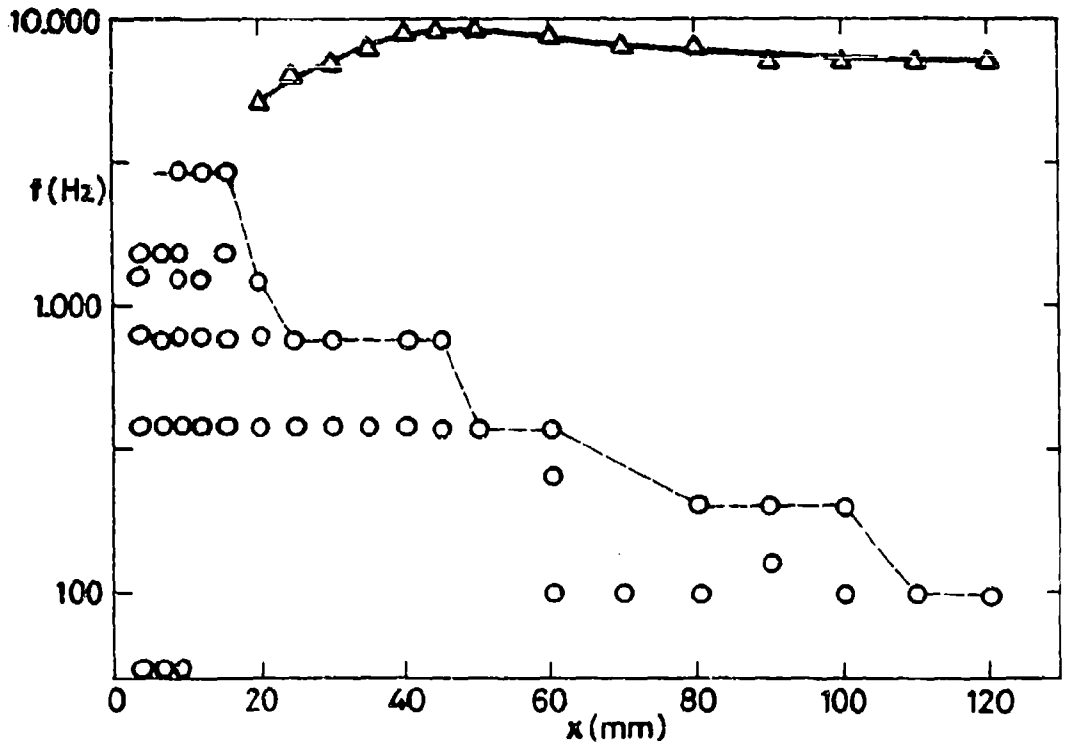

Fig. 12b.- For legend see page 43.

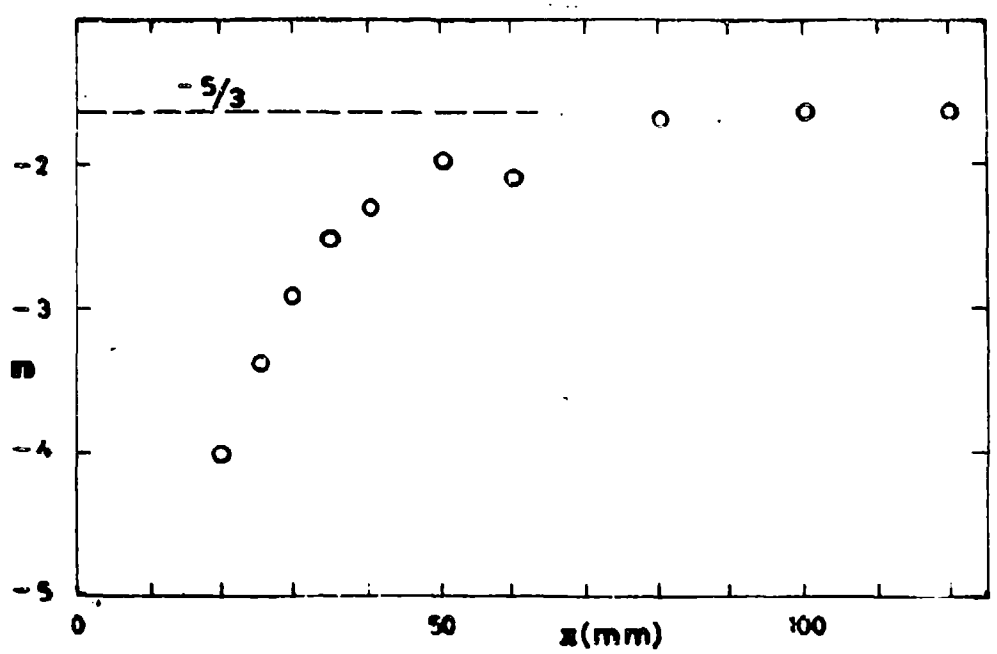

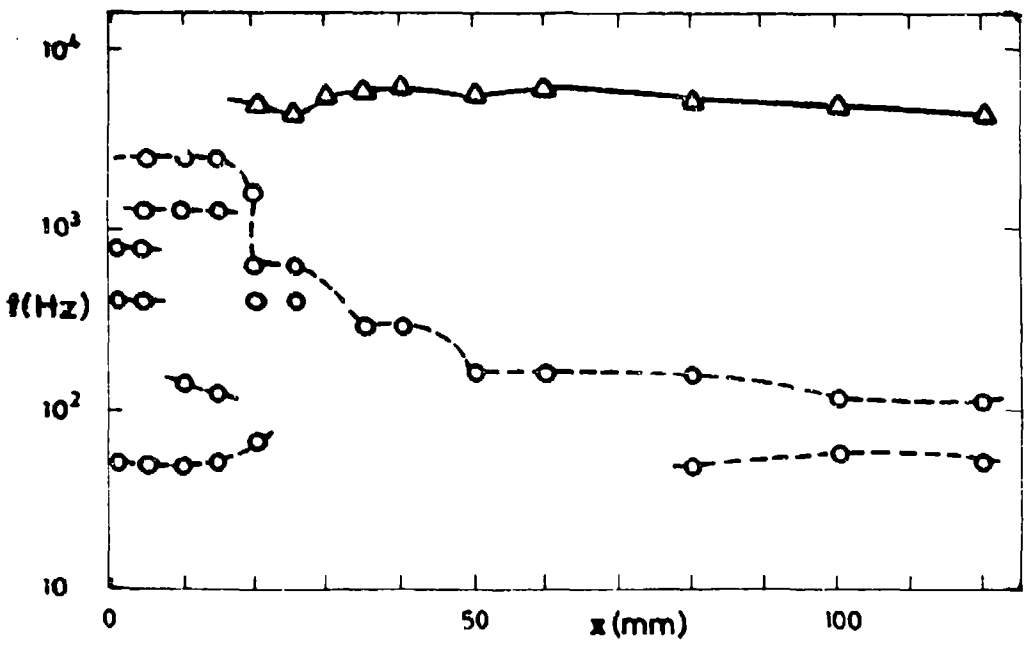

Fig. 12c.- For legend see page 43.

Fig. 12a, b, c.- Evolution of the frequency of the spectral peaks corresponding to large scales (o), and the frequency of the "nose" marking the end of the inertial range (Δ). Also slope of the inertial range. a) Water layer; b) Air (25 m/s); c) Air (16.4 m/s).

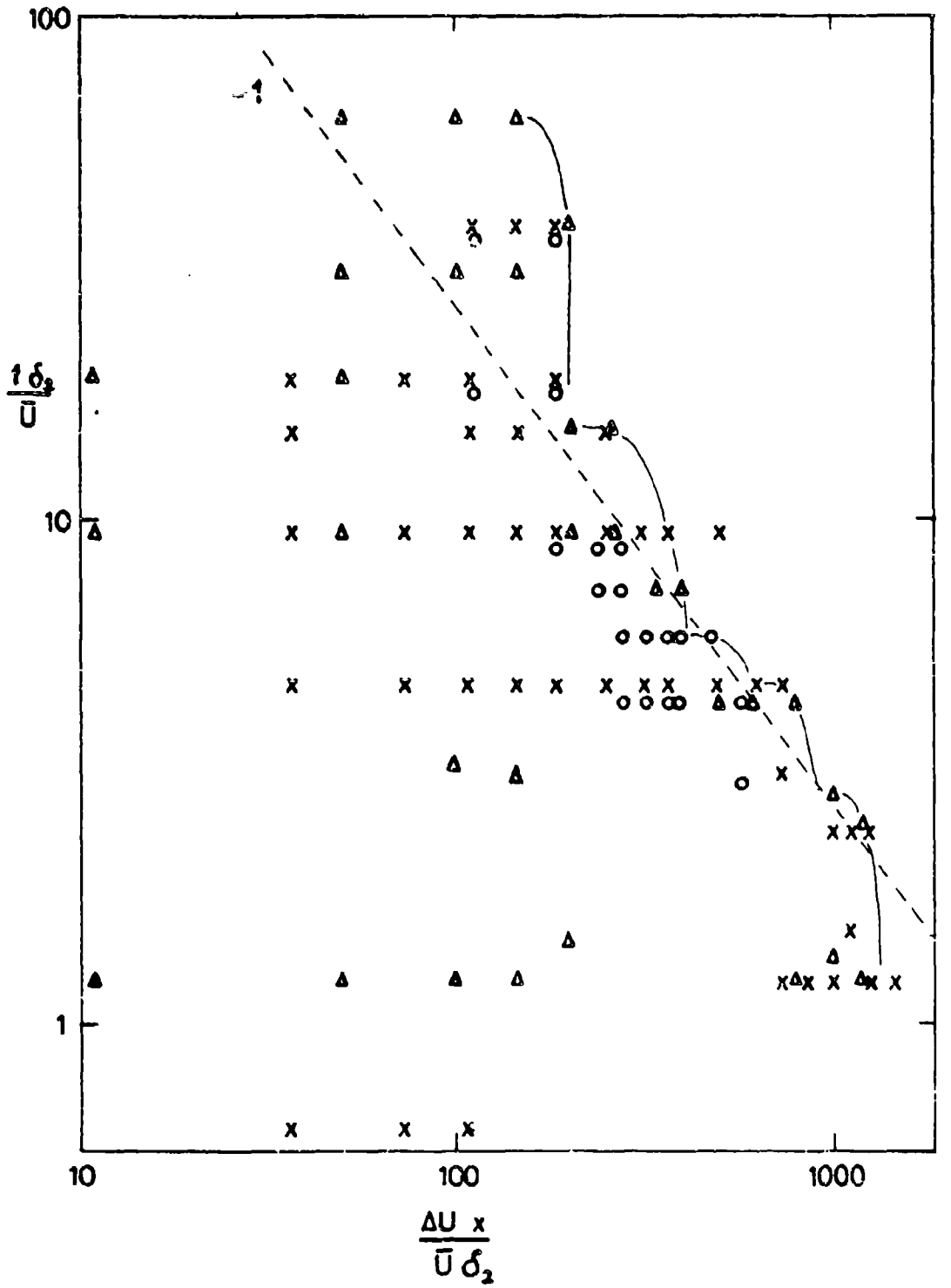

Fig. 13.- Dimensionless representation of large scale frequencies versus downstream coordinate. O , water; X , Air (25 m/s); Δ , Air (16.4 m/s).

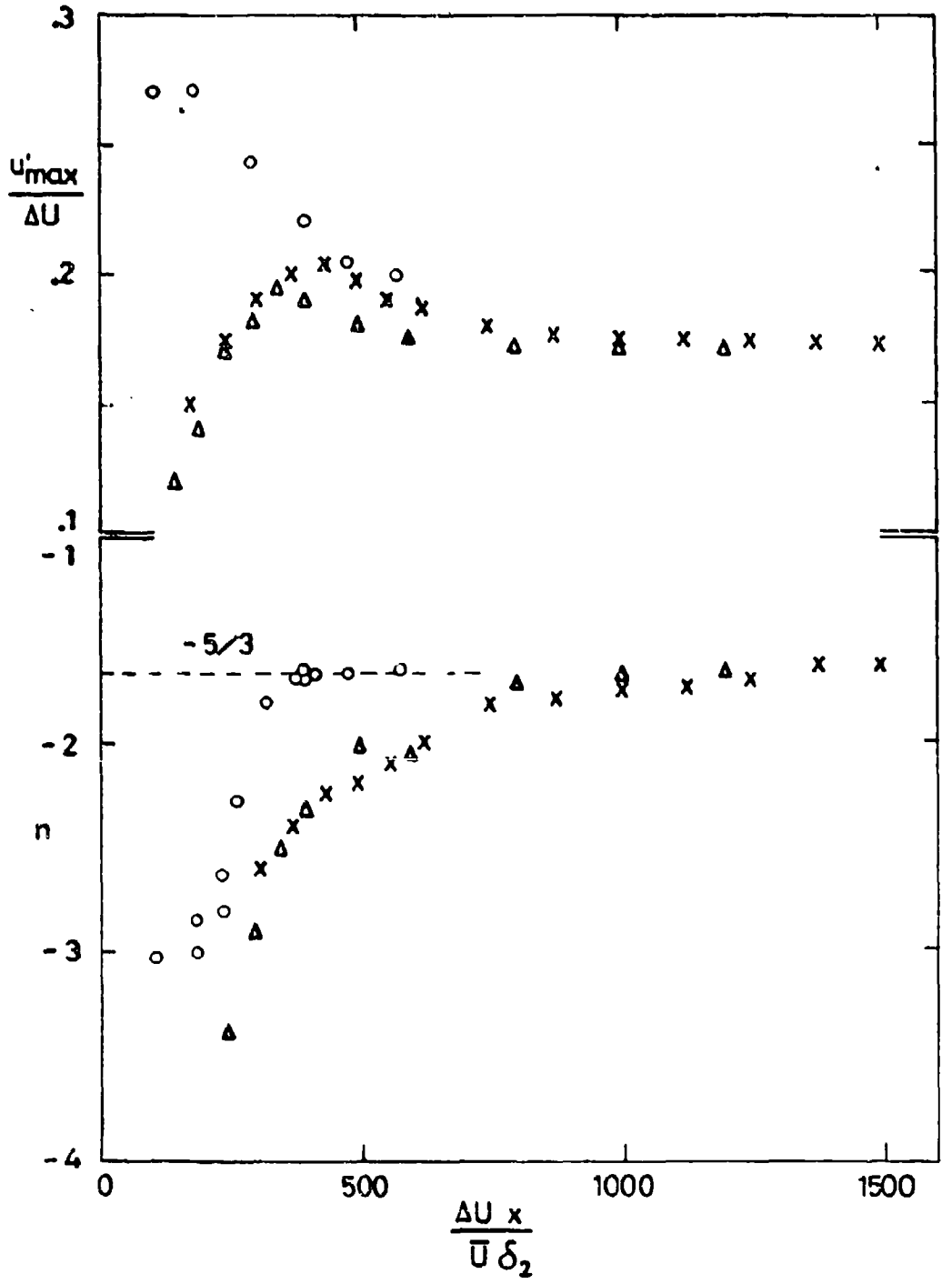

Fig. 14.- Dimensionless evolution of turbulence level (top) and slope of inertial subrange. O , water; X , Air (25 m/s); Δ , Air (16.4 m/s).

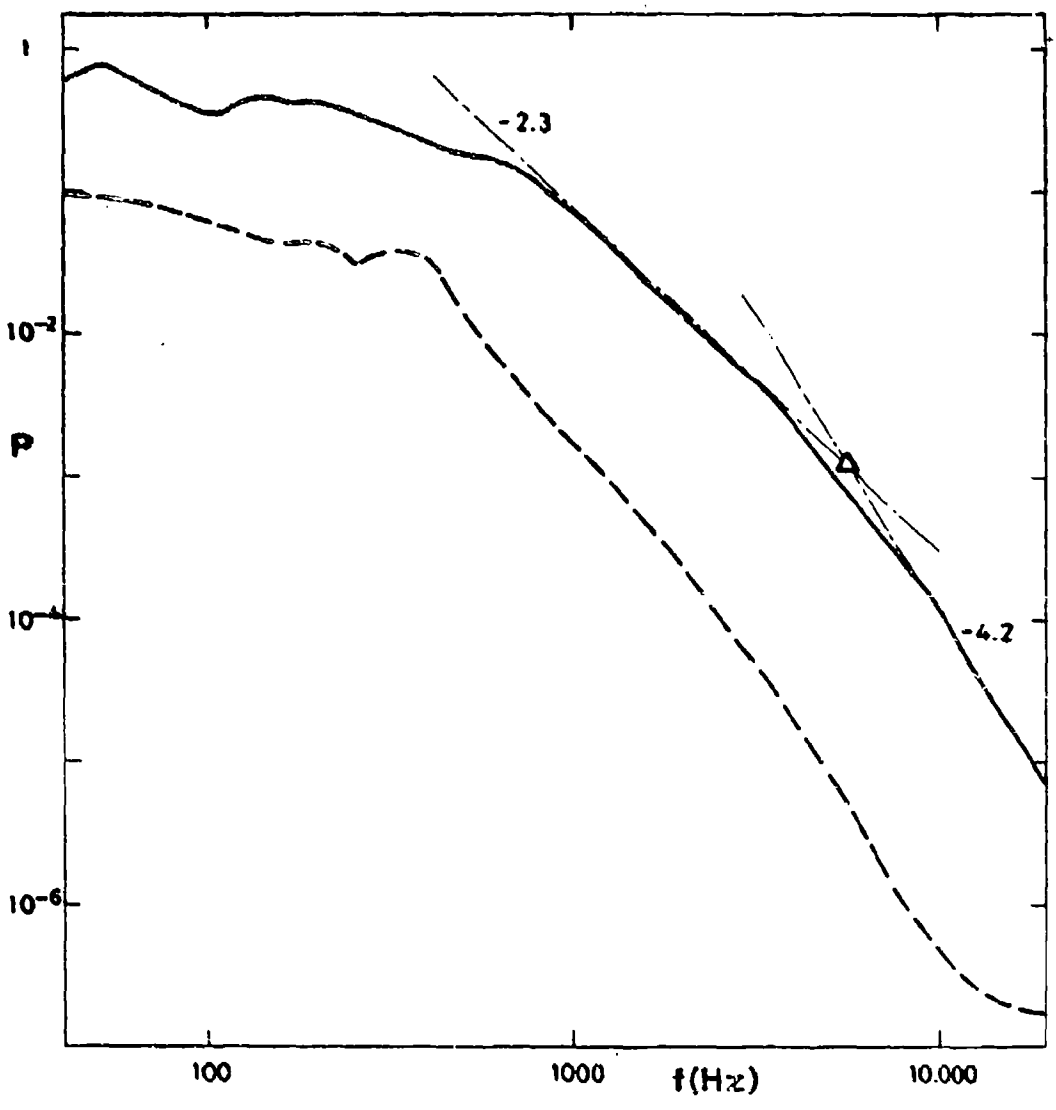

Fig. 15.- Definition of the inertial and probe-limited ranges in the power spectrum, showing the "nose" separating them.

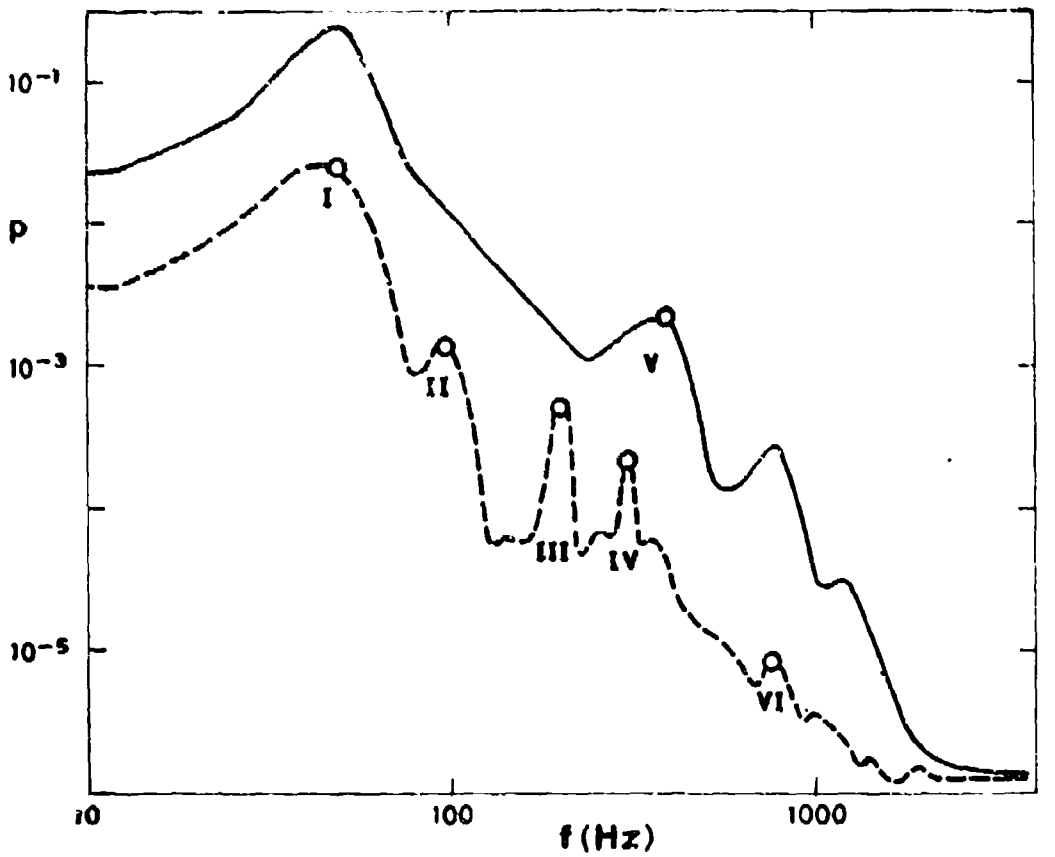

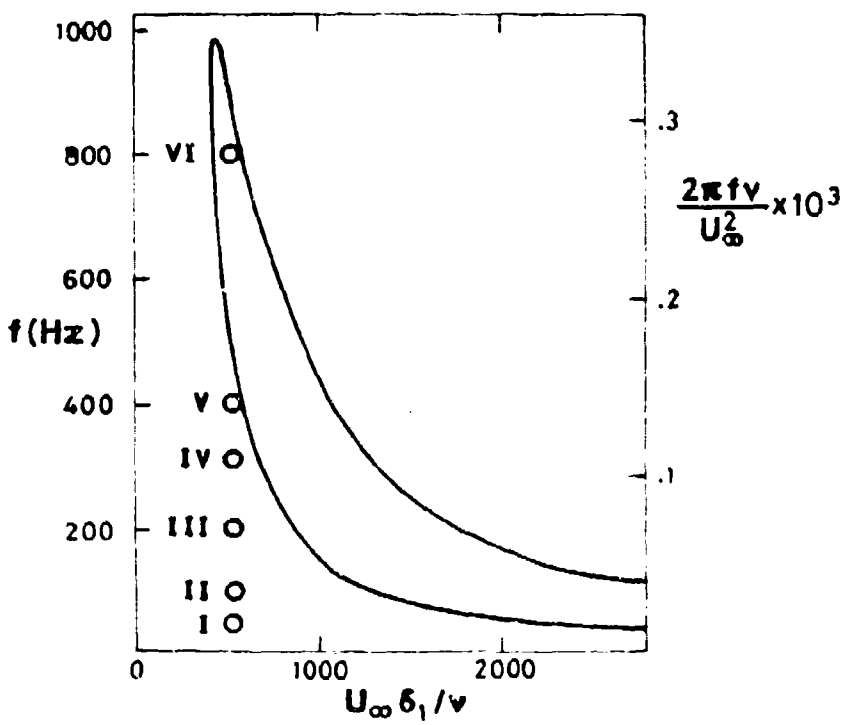

Fig. 16.- Power spectra of free stream (---) and boundary layer (—) measured at x = 1 mm, U/U∞ = .5. Significant peaks are represented on Tollmien's stability diagram for the laminar boundary layer. Layer II, z = 0.

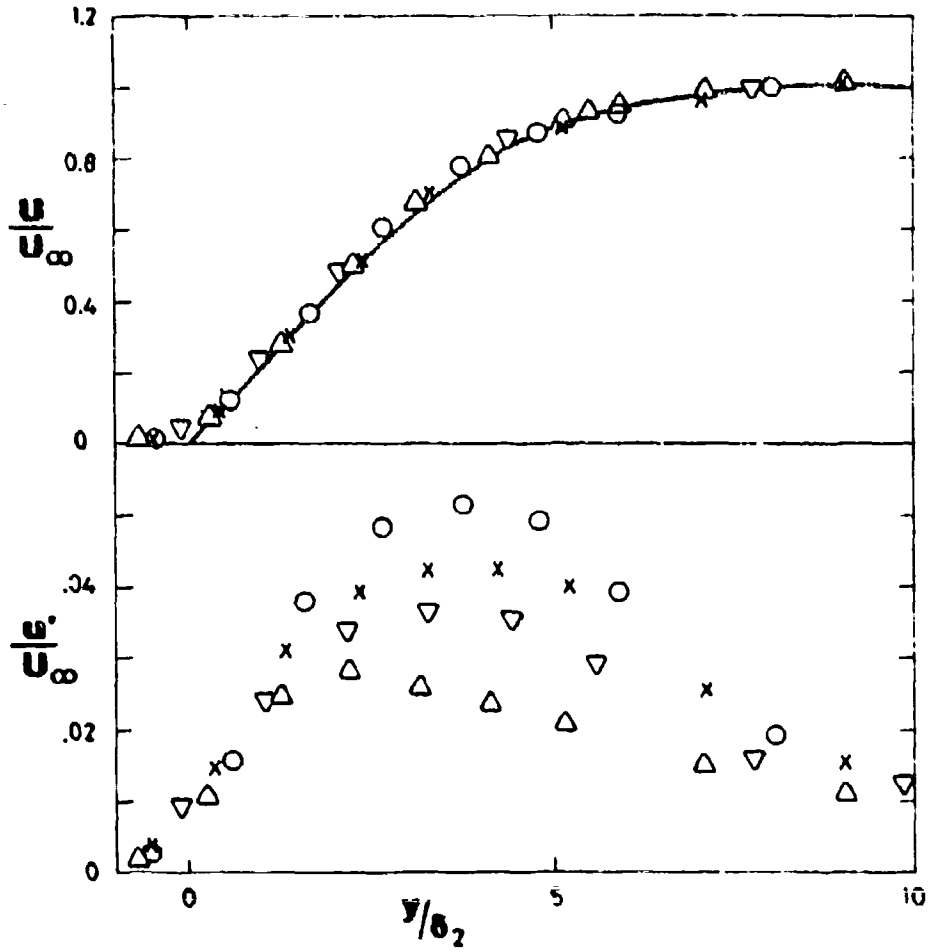

Fig. 17.- Nondimensional profiles of boundary layer at several spanwise locations. ○ , z = -35 mm; X , z = -25; ▽ , z = 15; △ , z = -5. Solid line is Blasius profile. Layer II, x = 1 mm.

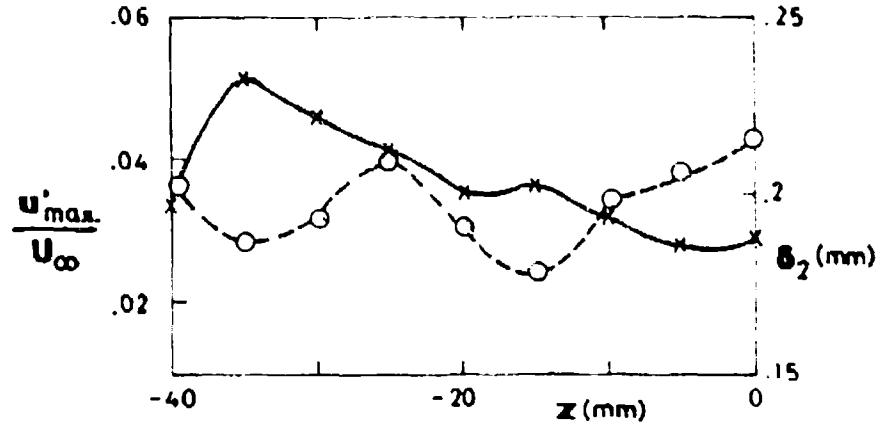

Fig. 18.- Spanwise variation of maximum turbulence level (——) and momentum thickness (----) for boundary layer. Layer II, x = 1 mm.

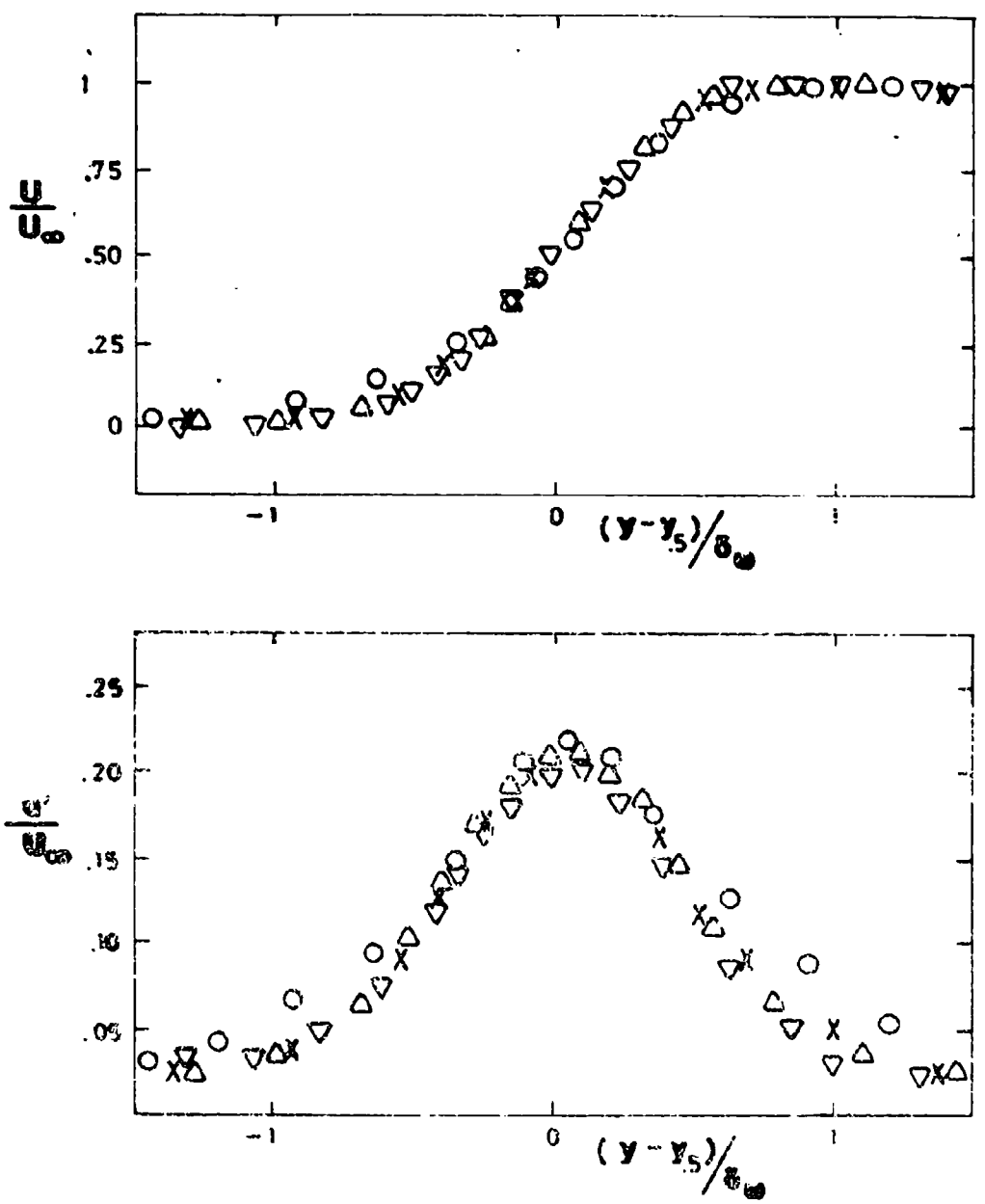

Fig. 19.- Nondimensional longitudinal velocity and trubulence level profiles. For the air layer. ○ , x = 40 mm; X , x = 60; Δ , x = 80; ▽ , x = 100. Layer I, z = 0; U_∞ = 16.4 m/s.

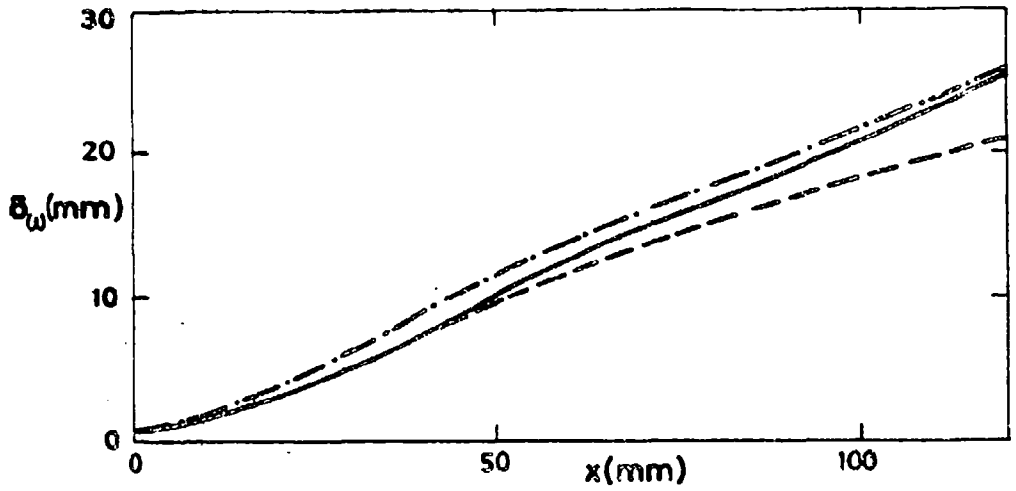

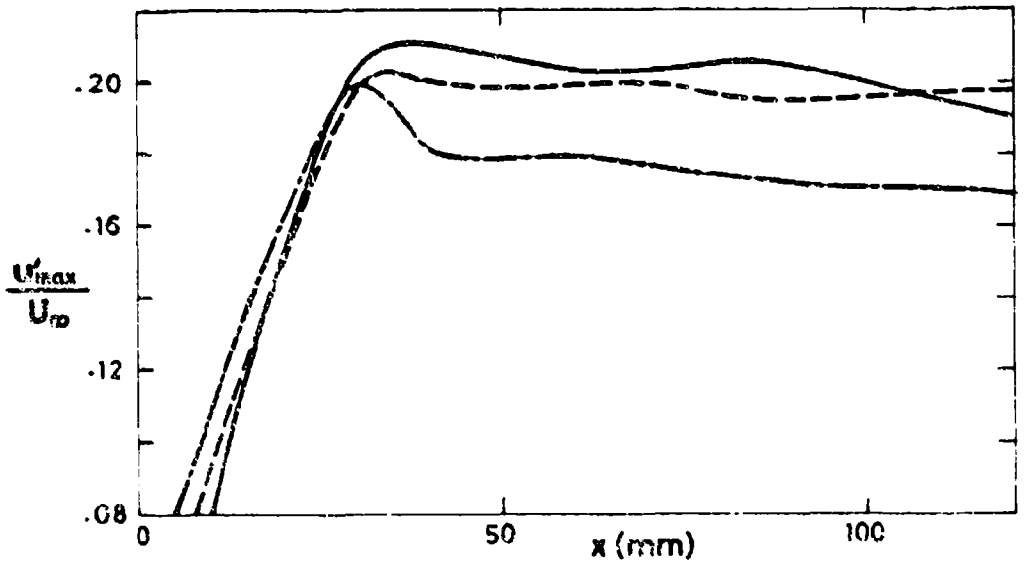

Fig. 20.- Vorticity thickness and maximum turbulence levels for three layers in air U_∞ = 16.4 m/s in all cases. —— I, z = 0; ----- I, z = 35 mm; -·-·- II, z = 0.

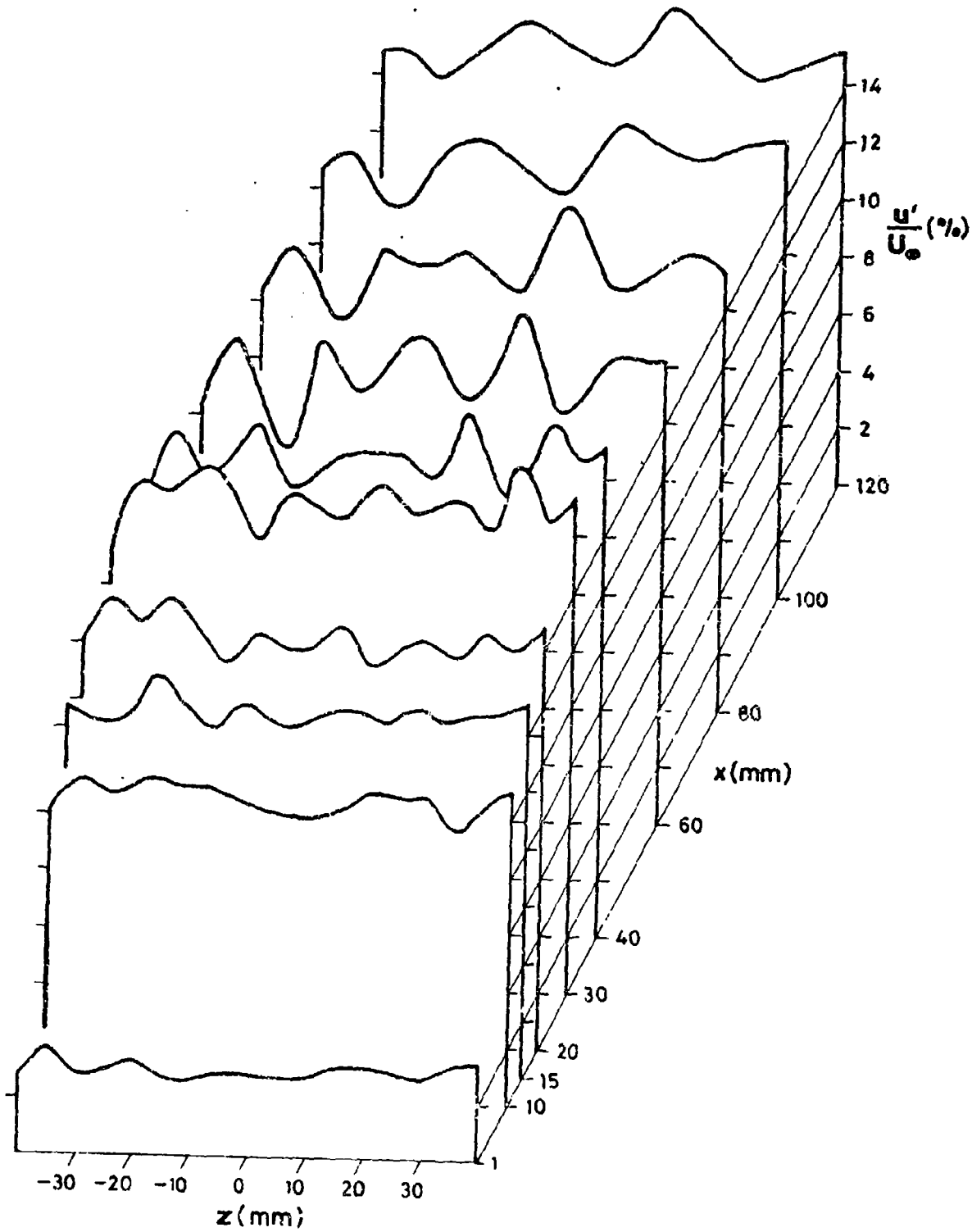

Fig. 21.- Turbulence level as function of streamwise and spanwise (z) coordinates. Figure corresponds to lower part of figure 23 and its position in the layer is marked in figure 22.

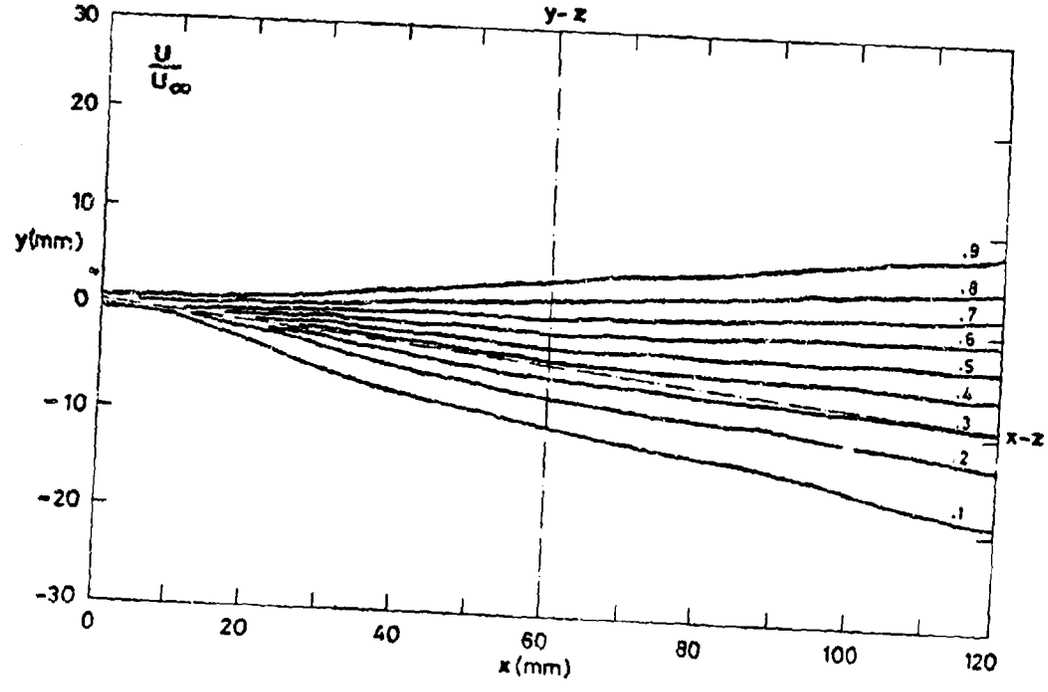

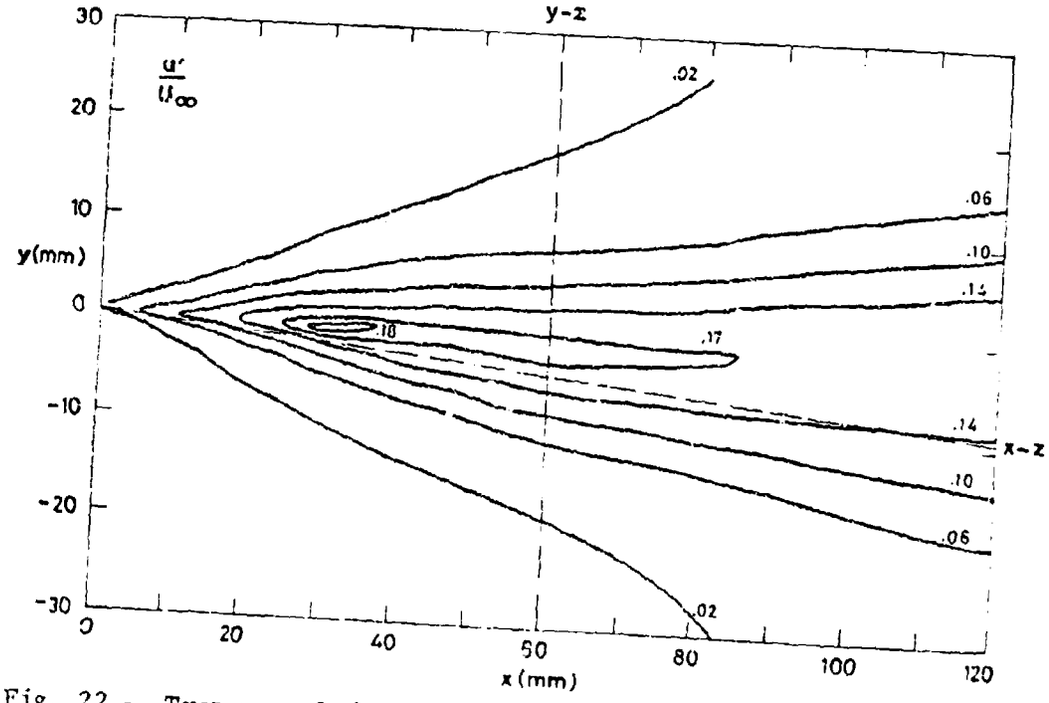

Fig. 22.- Transversal (x-y) maps of mixing layer at center of span. Configuration II, $z = 0$.

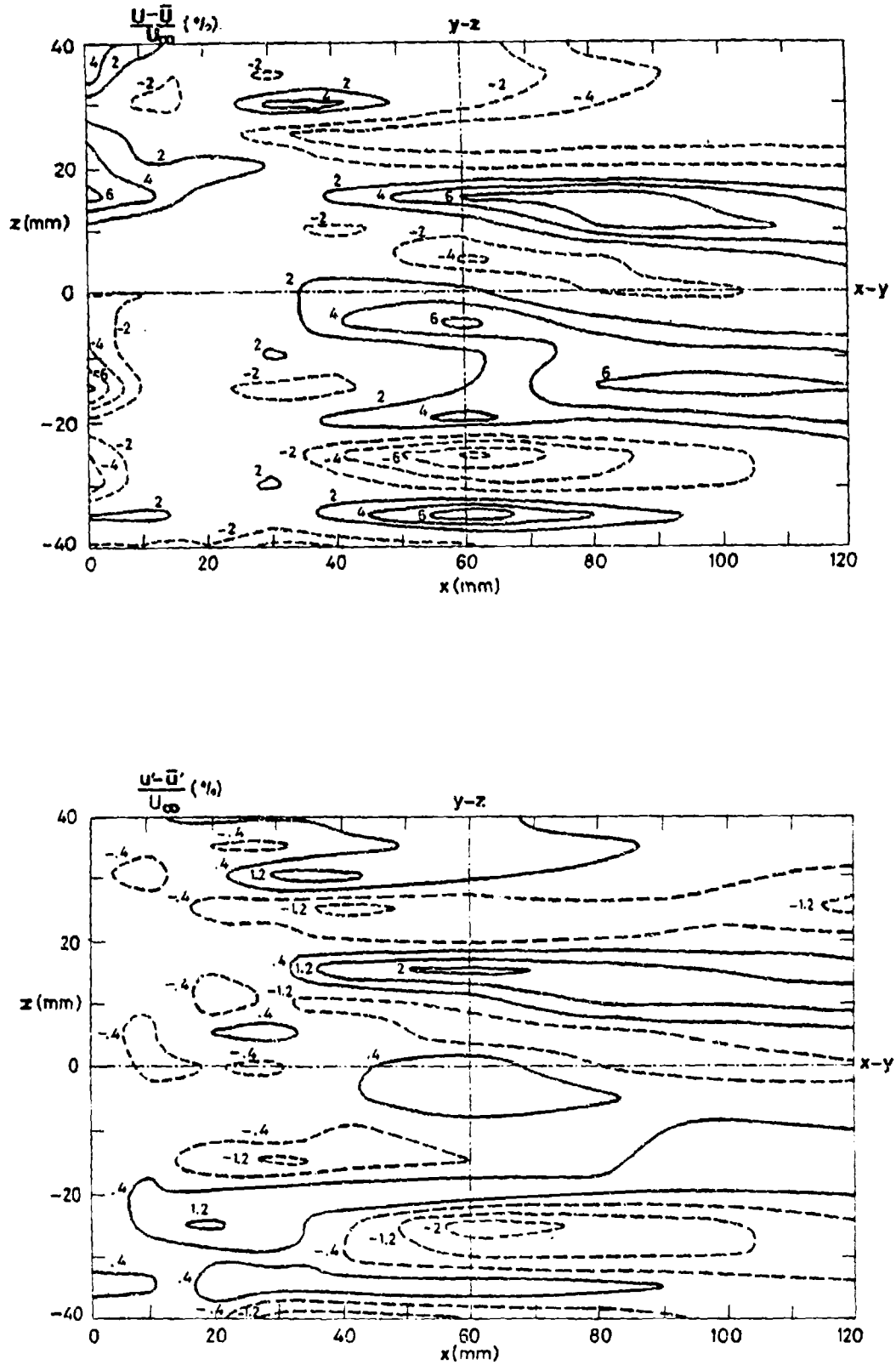

Fig. 23.- Longitudinal (x-z) maps of velocity and turbulence level deviations from spanwise uniformity. Configuration II; position of map defined in figure 22.

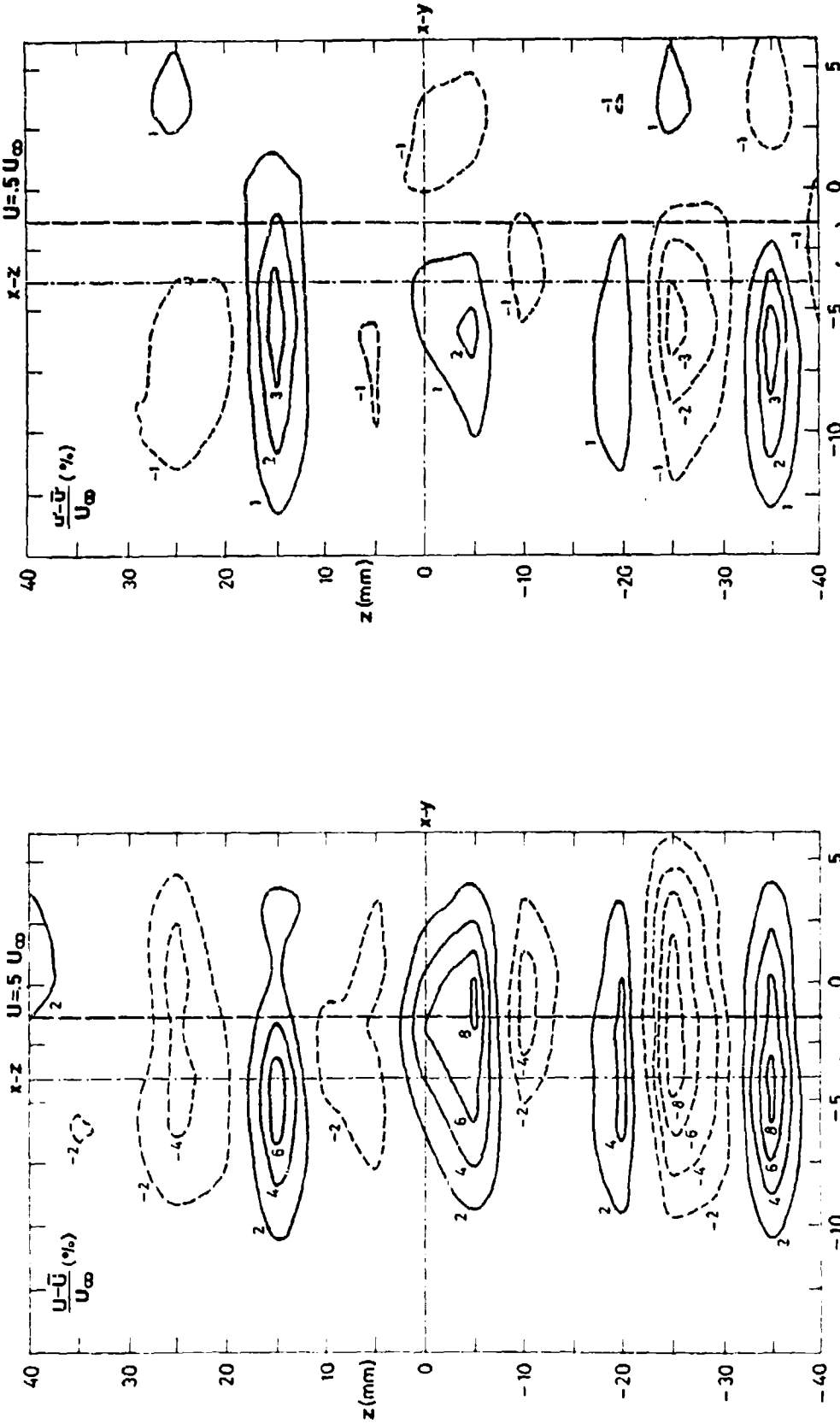

Fig. 24.- Transversal (y-z) maps of velocity and turbulence level deviations from spanwise uniformity. Configuration II, x = 60 mm.

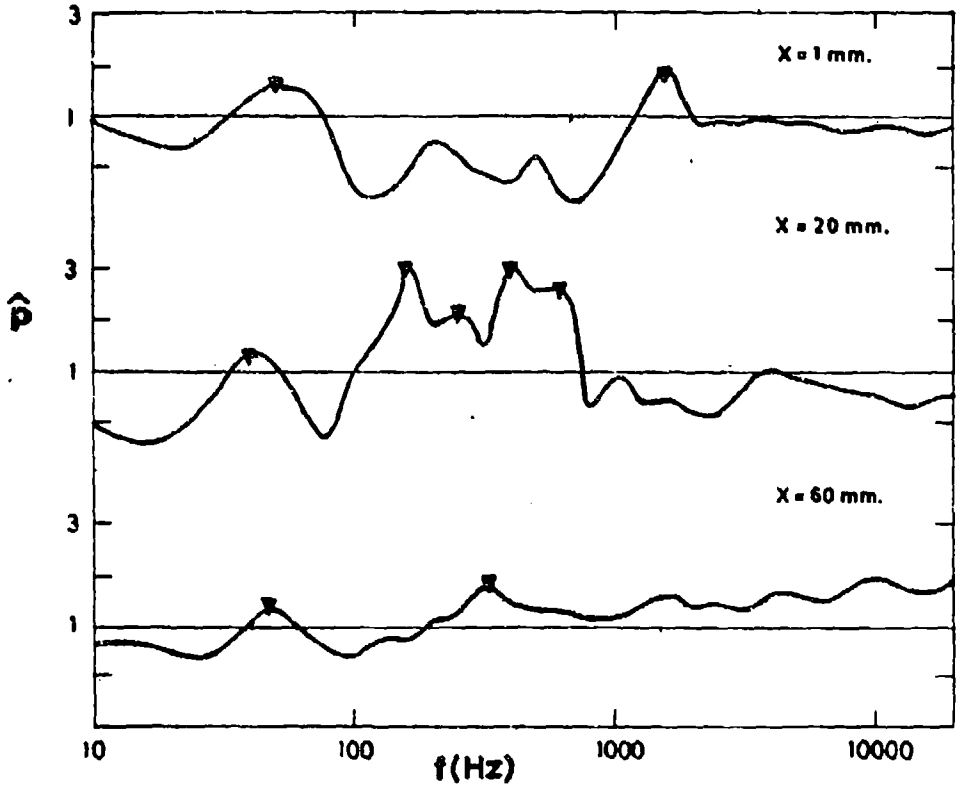

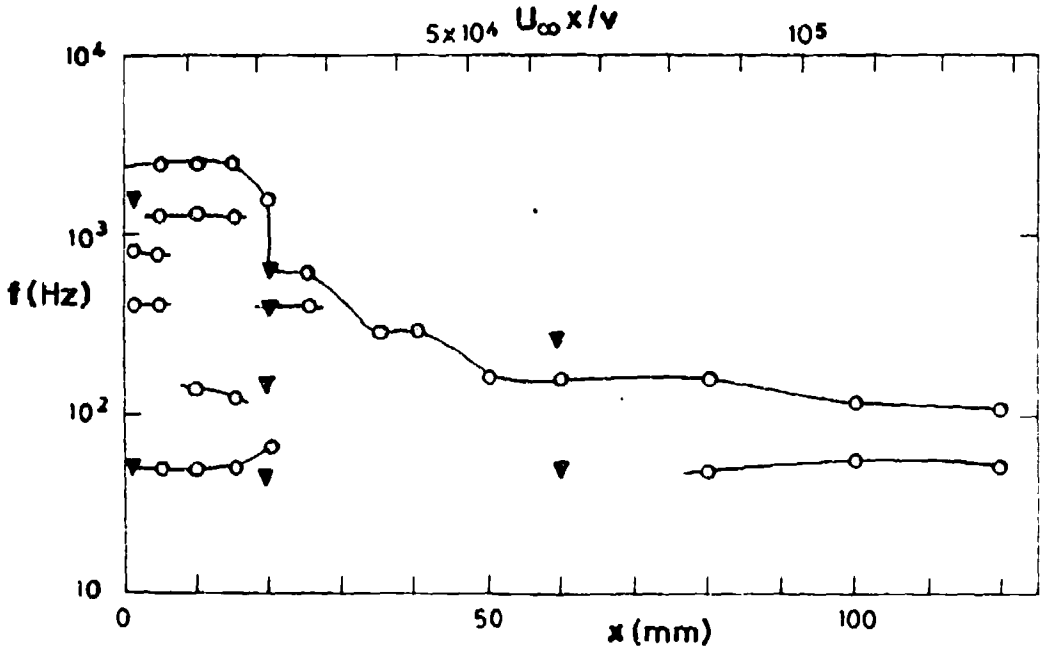

Fig. 25.- For legend see next page.

Fig. 26.- Normalized deviation of power spectra from spanwise uniformity; $\hat{p}$ defined in text. Each curve is average of several z positions. x = 1, y = .05 mm: z = -40,-30, -15, 10, 20, 35 mm; x = 20, y = -.9 mm: z = -35, -25, -15, 5, 10, 25, 40 mm; x = 60, y = -6 mm: z = -40, -35, -25, -20, -10, -5, 5, 15, 25mm. Spectral peaks are overlaid on frequency diagram for layer, (see figure 12c) to show relation to dominant peaks in the spectrum.

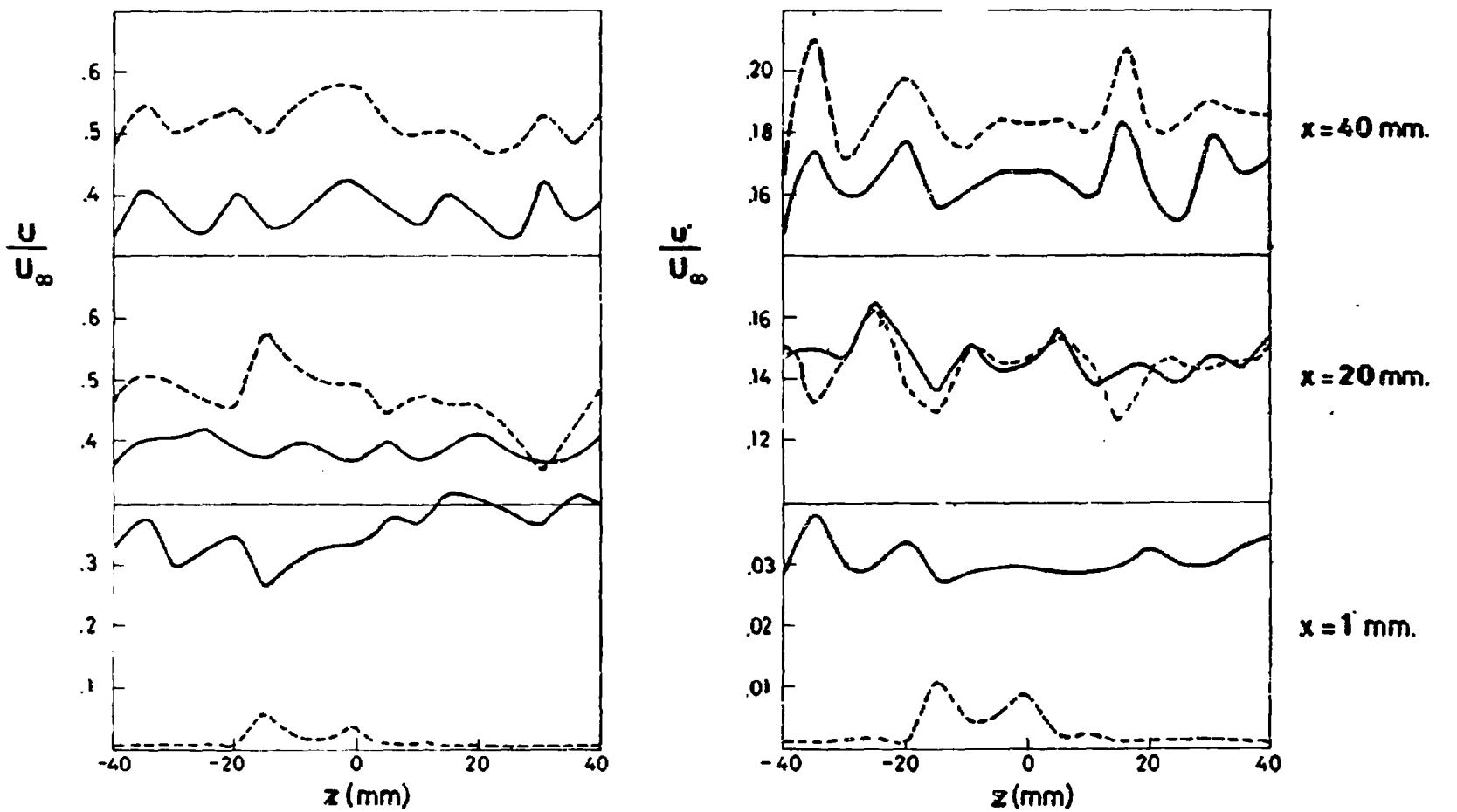

Fig. 26.- Average velocity and turbulence level at several spanwise traversings in two different mixing layer configurations. --- layer I;— II. See text regarding expected accuracy of measurements. All measurements in I are taken at y = 0. For layer II: x = 1, y=.2; x = 20, y = -.5; x = 40, y=-2.35.

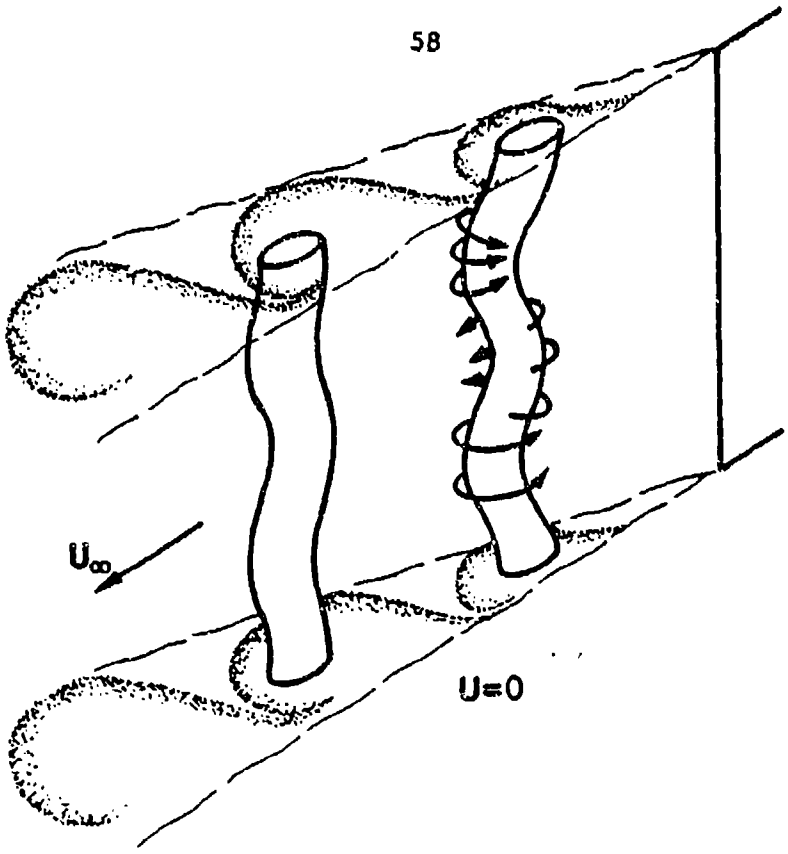

Fig. 27.- The corrugations of the vortex cores cause displacement of the turbulence level and variations in mean velocity.

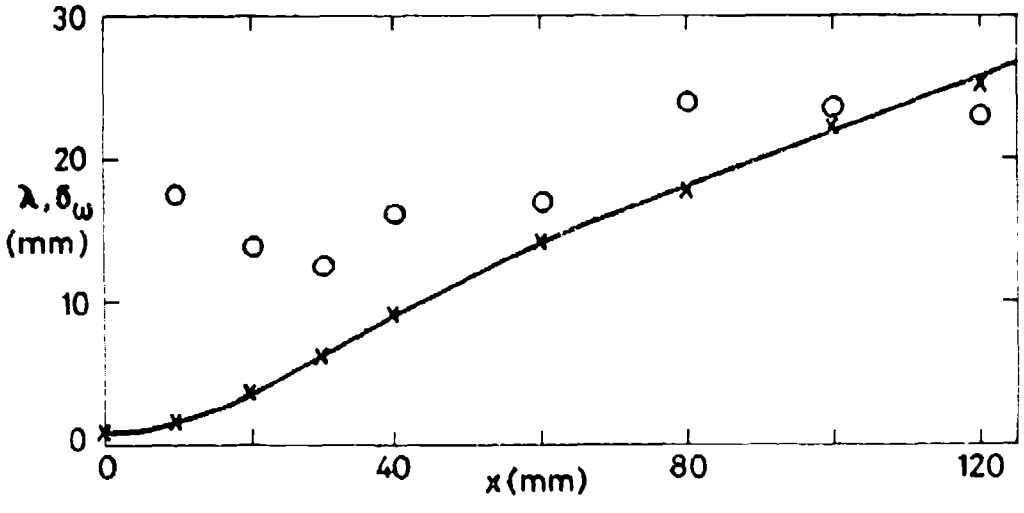

Fig. 28.- Spanwise wavelength of jet system in air layer. O , wavelength; solid line is vorticity thickness.

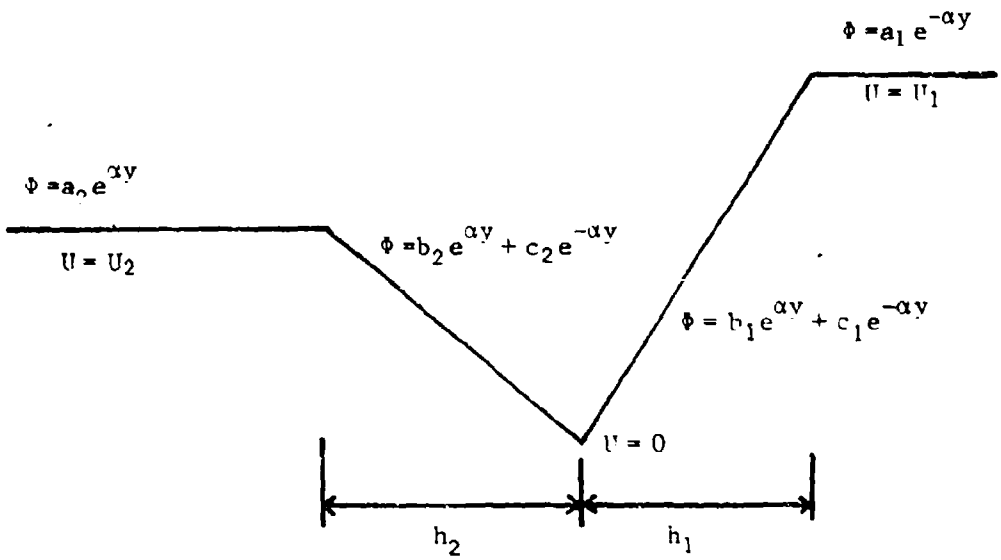

Fig. 29.- Straight line approximation for the wake profile of the splitter plate. Expressions are the perturbation amplitudes for the stream function.

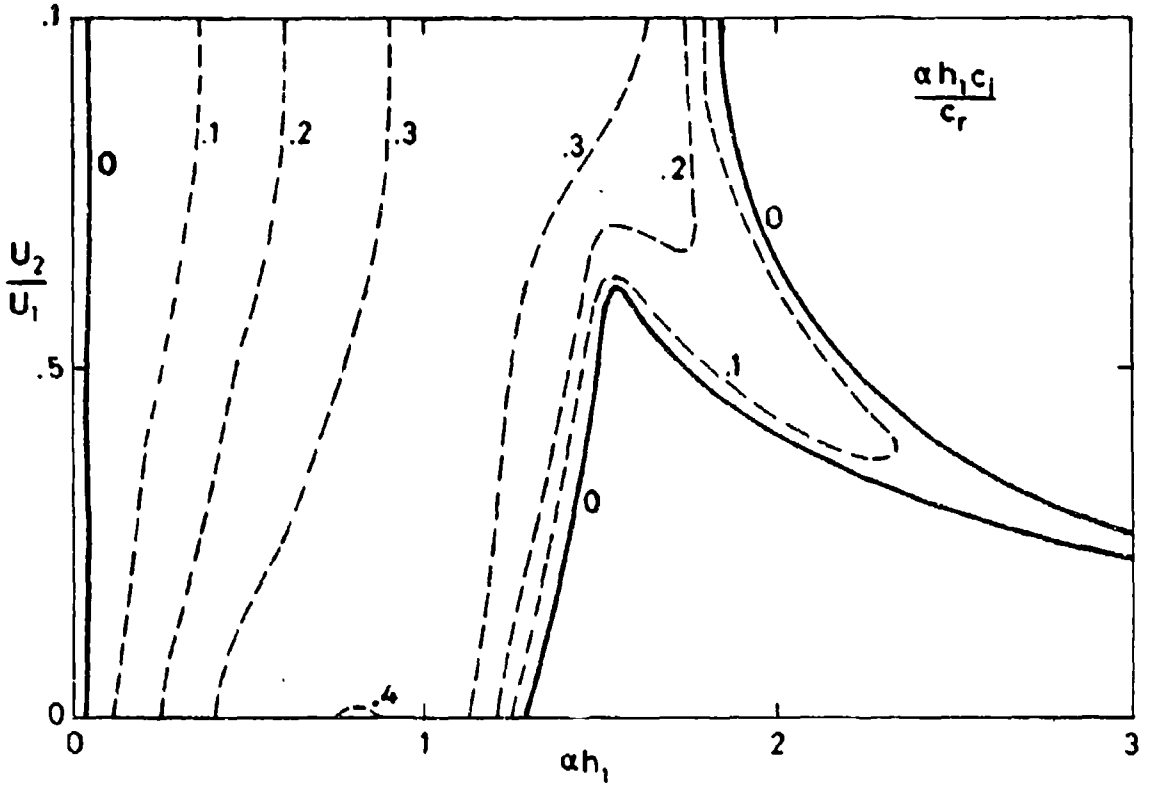

Fig. 30.- Spatial amplification rates and stability boundary for splitter plate wake when equivalent plate length is the same at both sides.

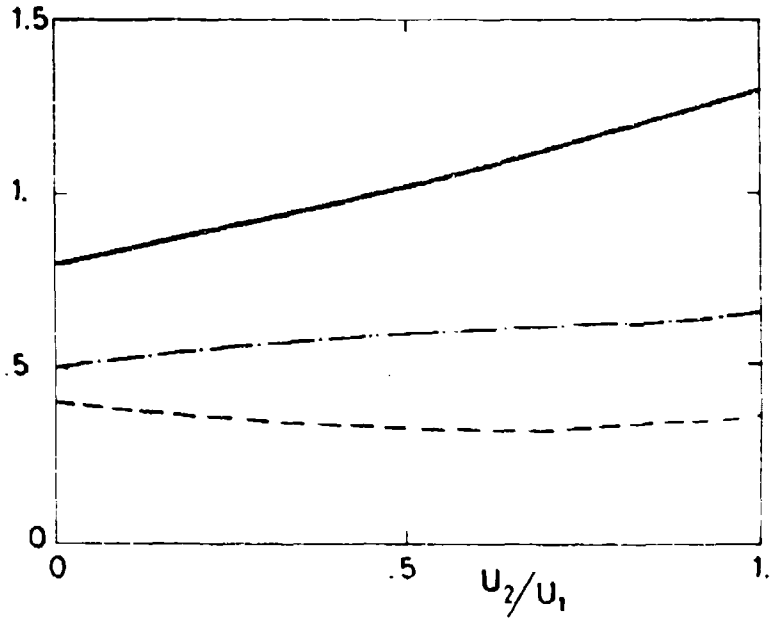

Fig. 31.- Properties of most spatially amplified wave above. —— αh_1; — · — · c_r/U_1; - - - - $\alpha h_1\ c_i/c_r$.